



ADA 085476

SECURITY CLASSIFICATION OF THIS PAGE (When Data Entered)

REPORT DOCUMENTATION PAGE		READ INSTRUCTIONS BEFORE COMPLETING FORM
1. REPORT NUMBER NRL Memorandum Report 4198	2. GOVT ACCESSION NO. AD-A085476	3. RECIPIENT'S CATALOG NUMBER
4. TITLE (and Subtitle) MAGNETO-OPTIC MATERIALS FOR BIASING RING LASER GYROS - Report No. 2 A063074	5. TYPE OF REPORT & PERIOD COVERED Interim report on a continuing NRL problem	
	6. PERFORMING ORG. REPORT NUMBER	
7. AUTHOR(s) G.A. Prinz, J.J. Krebs, W.G. Maisch and D.W. Forester	8. CONTRACT OR GRANT NUMBER(s)	
9. PERFORMING ORGANIZATION NAME AND ADDRESS Naval Research Laboratory Washington, DC 20375	10. PROGRAM ELEMENT, PROJECT, TASK AREA & WORK UNIT NUMBERS 6272N; WF21-234; 52-0821-0-0	
11. CONTROLLING OFFICE NAME AND ADDRESS Department of the Navy Naval Air Systems Command Washington, DC 20361	12. REPORT DATE April 14, 1980	
	13. NUMBER OF PAGES 46	
14. MONITORING AGENCY NAME & ADDRESS (if different from Controlling Office)	15. SECURITY CLASS. (of this report) UNCLASSIFIED	
	15a. DECLASSIFICATION/DOWNGRADING SCHEDULE	
16. DISTRIBUTION STATEMENT (of this Report)  Approved for public release; distribution unlimited.		
17. DISTRIBUTION STATEMENT (of the abstract entered in Block 20, if different from Report)		
18. SUPPLEMENTARY NOTES  This program is supported by NAVAIRSYSCOM through ADPO-35 on Contract N00019-80-WR-01055		
19. KEY WORDS (Continue on reverse side if necessary and identify by block number)  LPS Vol-4 Laser gyros Magneto-optical materials		
20. ABSTRACT (Continue on reverse side if necessary and identify by block number)  A series of new materials including alloys of transition metals (Fe, Co) with rare earths (Gd, Tb) have been fabricated and characterized. Analysis is provided of ellipsometric techniques used to obtain the magneto-optic properties. An improved definition of Figure-of-Merit for transverse Kerr effect mirror application.		

DD FORM 1473

JAN 73

EDITION OF 1 NOV 68 IS OBSOLETE  
S/N 0102-014-6601

i

SECURITY CLASSIFICATION OF THIS PAGE (When Data Entered)

TABLE OF CONTENTS

	Page
I. Introduction.....	1
II. Techniques for Magneto-Optic Measurements.....	2
A. Measurement of $n, k$ .....	2
B. Transverse Kerr Effect.....	3
C. Polar Kerr Effect.....	5
III. Magneto-Optic Bias of Ring Laser Gyro.....	7
A. Magnetic Mirror Overlaid with a Dielectric Stack.....	8
B. Optimum Construction.....	9
C. Figure-of-Merit.....	11
IV. Properties of Metallic Magnetic Materials.....	13
A. Optical Properties	
1. Alloys of Rare-Earths and Transition Metals ( $\lambda = 0.63\mu\text{m}$ ).....	13
2. Selected Materials at $\lambda = 1.15\mu\text{m}$ .....	15
B. Figure-of-Merit.....	16
C. Magnetic Properties.....	18
V. Conclusions.....	21
A. Performance at $1.15\mu\text{m}$ vs. $0.63\mu\text{m}$ .....	21
B. Alloys of Rare-Earths and Transition Metals.....	22
C. Recommendations.....	22
References.....	23

**DTIC**  
**ELECTE**  
**S** JUN 17 1980 **D**  
**B**

ACCESSION for		
NTIS	White Section	<input checked="" type="checkbox"/>
DDC	Buff Section	<input type="checkbox"/>
UNANNOUNCED		<input type="checkbox"/>
JUSTIFICATION		
BY		
DISTRIBUTION/AVAILABILITY CODES		
Dist.	AVAIL. and/or	SPECIAL
A		

MAGNETO-OPTIC MATERIALS FOR BIASING  
RING LASER GYROS

I. Introduction

This is the second of a series of reports on magneto-optical materials for biasing ring laser gyros. The first report was principally concerned with magnetic alloys which could be easily switched in low fields and, when prepared as thin films, would possess a magnetic moment in the film plane. Such materials might be suitable for transverse Kerr effect mirrors. This second report deals with binary alloys of rare-earths and transition metals. It investigates the suitability of such alloys for fabricating polar Kerr effect mirrors in which a permanent magnetic moment exists normal to the film plane. Such mirrors would be useful, for example, in multi-oscillator ring gyros.

In addition to the properties of these specific materials, analysis is provided of the ellipsometric techniques used to obtain the materials' magneto-optic properties. There is also an improved definition of the Figure-of-Merit which is used to compare materials intended to be used in a transverse Kerr effect mirror application. Characterization of the most promising materials in Report No. 1 was extended by measurement of their magneto-optical properties at the infrared He-Ne laser wavelength  $1.15\mu\text{m}$ .

---

Work reported in this document was completed before 1 October 1979  
Manuscript submitted February 11, 1980

## II TECHNIQUES FOR MAGNETO-OPTIC MEASUREMENTS

In this section we give the mathematical justification for the methods we have used to make magneto-optic measurements on a wide variety of optically opaque thin film magnetic alloys. The experimental arrangements used for the transverse and polar Kerr effect measurements are shown in Figs. 1 and 2 and have been discussed in Report No. 1.<sup>1</sup>

### A. Measurement of $N = n-ik$

We recall that the complex Fresnel reflection coefficients  $r_{ij}$  are defined in terms of the s- and p-polarized amplitude components of the incoming ( $E_p, E_s$ ) and reflected ( $R_p, R_s$ ) beams by the equation

$$\begin{pmatrix} R_p \\ R_s \end{pmatrix} = \begin{pmatrix} r_{pp} & r_{ps} \\ r_{sp} & r_{ss} \end{pmatrix} \begin{pmatrix} E_p \\ E_s \end{pmatrix} . \quad (\text{II-1})$$

The ellipsometric parameters  $\psi$  and  $\Delta$  are defined by the equation

$$r_{pp}/r_{ss} \equiv (\tan \psi)e^{i\Delta} \quad (\text{II-2})$$

where  $\psi$  and  $\Delta$  are real. Their name comes from the fact that they are directly determined in a standard ellipsometric measurement of opaque thin films.

For a detailed discussion of the ellipsometric methods for determining  $n$  and  $k$ , the real and imaginary parts of the complex index of refraction  $N = n-ik$  of such a film, we refer the reader to the excellent manual by Archer<sup>2</sup> which is oriented toward the Gaertner ellipsometer used in this work. It is shown there for a non-magnetic, isotropic, opaque film (i.e. with  $r_{ps} = r_{sp} = 0$ ), that the intensity  $I$  which reaches the ellipsometer detector in Fig. 1 is given by

$$I = I_{\min} + I_0 [\sin^2(\psi + \bar{A}) - (\sin 2\bar{A} \sin 2\psi) \sin^2 \frac{1}{2}(\Delta + \Delta')] \quad (\text{II-3})$$

where  $I_0$  is the incident intensity,  $I_{\min}$  is the minimum intensity (due to imperfect polarizers, scattering, etc.),  $\bar{A}$  is the analyzer angle setting and  $\Delta'$  is related to the polarizer angle  $P$  by  $\Delta' = 90^\circ - 2P$ .

Once the analyzer and polarizer scales are calibrated<sup>2</sup> one can determine  $\psi$  and  $\Delta$  by searching for the deep minima (nulls) in  $I$ . There are two distinct minima, one at ( $\bar{A} = -\psi$ ,  $\Delta' = -\Delta$ ) and the other at ( $\bar{A} = \psi$ ,  $\Delta' = 180^\circ - \Delta$ ). This permits a useful cross check on the values determined and allows one to eliminate errors. Once  $\psi$  and  $\Delta$  are known,  $n$  and  $k$  can be found by means of rather messy equations involving the angle of incidence  $\phi$ . The explicit equations appear in Archer<sup>2</sup> (Eqs. 34-36) and were used in our own work to determine  $n$  and  $k$  for the magnetic films studied.

### B. Transverse Kerr Effect

Our transverse Kerr method for measuring the complex magneto-optical coefficient  $Q = Q_1 - iQ_2$  is based on the fact that changing the state of transverse magnetization changes the values of  $\psi$  and  $\Delta$  as shown below. We recall<sup>1</sup> that for a magnetized sample in the transverse Kerr configuration the Fresnel coefficients are given by

$$\begin{aligned} r_{pp} &= r_{pp}^0(1+QA), & r_{ss} &= r_{ss}^0 \\ r_{sp} &= r_{ps} = 0 \end{aligned} \quad (\text{II-4})$$

where a superscript zero implies the demagnetized state. The complex quantity  $A$  has been defined before (Eq. IV-2, Report No. 1).

Since  $|Q| \ll 1.0$  we can restrict ourselves to first order terms in  $Q$  which are proportional to the sample magnetization  $M$ . When the sample is magnetized then

$$\tan\psi(\vec{M})e^{i\Delta(\vec{M})} = (r_{pp}^0/r_{ss}^0)(1+QA). \quad (\text{II-5})$$

It is then easy to show that

$$\tan\psi(\vec{M}) = (\tan\psi_0) \{1 + \text{Re}(QA)\} \quad (\text{II-6})$$

and

$$\Delta(\vec{M}) = \Delta_0 + \text{Im}(QA) \quad (\text{II-7})$$

to first order in Q. Here  $\text{Re}(X)$  and  $\text{Im}(X)$  imply the real and imaginary parts of X.

We now define  $\delta\psi = \psi(M) - \psi_0$  and  $\delta\Delta = \Delta(M) - \Delta_0$ . Then from a Taylor series expansion we conclude that

$$\tan\psi(\vec{M}) = \tan\psi_0 + \delta\psi \sec^2\psi_0. \quad (\text{II-8})$$

Hence by comparing (II-6) and (II-8) we get

$$\text{Re}(QA) = 2 \delta\psi / \sin 2\psi_0, \quad (\text{II-9})$$

while (II-7) gives

$$\text{Im}(QA) = \delta\Delta. \quad (\text{II-10})$$

Since A can be calculated from  $\phi$ , n and k, we can determine Q from (II-9, 10) if we measure  $\delta\psi$  and  $\delta\Delta$ .

We used a method based on (II-3) involving redundant data to obtain  $\delta\psi$  and  $\delta\Delta$ . We first established a fiducial setting of the analyzer and polarizer at the null corresponding to  $\bar{A} = -\psi_0$ ,  $\Delta' = -\Delta_0$ . We next introduce a small offset  $\delta\bar{A}$  ( $\approx 2^\circ$ ) in  $\bar{A}$  and measure the intensity  $I(\delta\bar{A}, M=0)$  reaching the detector. For the same analyzer setting we measure I with the sample magnetically saturated in both the positive and negative directions, i.e. we measure  $I(\delta\bar{A}, +M)$  and  $I(\delta\bar{A}, -M)$ . The same set of measurements are then made for an analyzer offset  $-\delta\bar{A}$ , and for polarizer offsets  $+\delta P$  and  $-\delta P$ . These angular offsets are introduced to make the change in I more sensitive to the desired quantities  $\delta\psi$  and  $\delta\Delta$ . An analysis based on the above procedure and (II-3) allows one to determine  $\delta\psi$  and  $\delta\Delta$  entirely in terms of these measured intensities. The redundancy of the data tends to cancel systematic errors and to give accurate values for  $Q_1$  and  $Q_2$ . This transverse Kerr technique was used therefore to character-

ize all of the magnetically soft films.

While it is true that the absolute sensitivity of  $I$  to  $\delta\psi$  and  $\delta\Delta$  is improved by increasing  $|\delta\bar{A}|$  and  $|\delta P|$  beyond the range we used, the improvement is illusory. Temporal fluctuations in the laser intensity soon produce larger changes in  $I$  than those induced by magnetizing the sample. The optimum signal-to-noise ratio is achieved when  $\delta\bar{A}$  and  $\delta P$  are comparable to, but somewhat larger than,  $\delta\psi$  and  $\delta\Delta$ . It proved helpful to use a digital readout of the intensity, especially when the magnetization-induced changes were small. We used a large angle of incidence  $\phi = 70^\circ$  since the measurements of both  $N$  and  $Q$  are most sensitive for such angles. The absolute signs of  $Q_1$  and  $Q_2$  were determined by comparison to standard materials (Fe, Co, permalloy) with known signs.

Very<sup>3</sup> recently, Minden has given his own ellipsometric technique for measuring the magneto-optic coefficient  $Q$  using the transverse Kerr effect. His method uses a.c. modulation of the film magnetization together with lock-in methods to measure  $\delta(\tan\psi)/\tan$  ( $= 2\delta\psi / \sin 2\psi$ ) and  $\delta\Delta$  and to deduce  $Q_1$  and  $Q_2$  from these. Thus the philosophy behind his technique is identical to ours although the details of carrying the measurements are quite different. His method requires separate measurements of both the total intensity  $I$  and the a.c. component  $\delta I$  over a wide range of polarizer angle settings. While the use of a.c. lock-in techniques is perhaps more elegant than the d.c. method used here the total amount of time required to take the data may well be greater in the former method and the accuracy of the final results seems comparable.

### C. Polar Kerr Effect

The polar Kerr effect at normal incidence has been used to characterize any magnetic film which could not be saturated in our transverse Kerr apparatus. Again the experimental arrangement was described in Report No. 1 and we now briefly describe the analysis used to determine  $Q_1$  and  $Q_2$ . Based on Eq. IV-7' of Ref. 1 we can write the Fresnel equations for right (+) and left (-) circularly polarized light at normal incidence as

$$R^\pm = r^\pm E^\pm = |r^\pm| e^{i\Delta^\pm} E^\pm \quad (\text{II-11})$$

with

$$|r^\pm| = |r_{pp}^0| \{1 \mp \operatorname{Re}(BQ)\} \quad (\text{II-12})$$

$$\Delta^\pm = \mp \operatorname{Im}(BQ) \quad (\text{II-13})$$

and

$$B = N/(N^2-1). \quad (\text{II-14})$$

Now the Kerr rotation  $\theta_k$  and Kerr ellipticity  $\epsilon_k$  for this case are defined<sup>4</sup> by

$$\theta_k = -\frac{1}{2}(\Delta^+ - \Delta^-) \quad (\text{II-15})$$

$$\epsilon_k = -\{ |r^+| - |r^-| \} / \{ |r^+| + |r^-| \} \quad (\text{II-16})$$

Hence we have

$$\theta_k = \operatorname{Im}(BQ) \quad (\text{II-17})$$

and

$$\epsilon_k = \operatorname{Re}(BQ) \quad (\text{II-18})$$

Hence a measurement of  $\theta_k$  and  $\epsilon_k$  allows one to deduce  $Q_1$  and  $Q_2$  if  $n$  and  $k$  are known from previous ellipsometer measurements.

In Fig. 2 we adjust the quarter-wave plate to have its axis vertical. Polarizer angles are measured from a vertical reference and analyzer angles from a horizontal one. For a small polarizer angle  $P$  the beam which reaches the sample will have an ellipticity  $\epsilon = P$ . We adjust both  $P$  and  $\bar{A}$  to achieve a null, first in a positive and then in a negative magnetic field. In this measurement the Kerr ellipticity is exactly cancelled by that induced by the setting of  $\bar{P}$  while the Kerr rotation is measured by the setting of  $\bar{A}$  required to achieve a null. If we define  $\delta P \equiv P(M) - P(-M)$  and  $\delta \bar{A} \equiv \bar{A}(M) - \bar{A}(-M)$ , then it is easy to show that

$$\theta_k = \operatorname{Im}(BQ) = -\frac{1}{2} \delta \bar{A} \quad (\text{II-19})$$

and

$$\epsilon_k = \text{Re}(BQ) = -\frac{1}{2} \delta P. \quad (\text{II-20})$$

The accuracy of determining  $\theta_k$  and  $\epsilon_k$  is essentially given by how accurately we can measure  $\delta \bar{A}$  and  $\delta P$ . The accuracy achieved is  $\pm 0.02^\circ$  for  $\delta \bar{A}$  and  $\delta P$ . To give some perspective to these numbers we note that for pure cobalt films  $\delta \bar{A} = -0.70^\circ$  and  $\delta P = -0.18^\circ$ .

### III. MAGNETO-OPTIC BIAS OF RING LASER GYRO

The principal requirements of a magneto-optic (M-0) element in a ring laser gyro (RLG) are:

- 1) adequate differential phase shift (bias);
- 2) low optical loss.

Hence it is reasonable to use the ratio of the differential phase shift to the optical loss as the primary Figure-of-Merit for a RLG M-0 element and we will consider this in more detail below. In any given application there are also other important factors such as ease of phase shift reversal, thermal stability of the phase shift, freedom from unwanted transients, etc. Nevertheless, no M-0 element can be considered useful for RLG use unless it has an adequate Figure-of-Merit.

Let  $\phi$  be the relative phase shift due to the M-0 effect between two counter-propagating beams in a ring laser. As a result the beams will see optical paths of slightly different optical lengths and hence will operate at slightly different wavelengths (and frequencies). The frequency difference  $\Delta \nu$  is related to  $\phi$  by the simple formula

$$\Delta \nu = (c/L) (\phi / 2\pi) \quad (\text{III-1})$$

where  $c$  is the velocity of light and  $L$  is the optical length of the ring laser.

In an RLG this frequency difference can be used to provide the bias required to avoid lock-in at low rotation rates. In practical ring laser gyroscopes typical required values are  $(\Delta \nu)_{\text{min}} = 50 - 100$  kHz. Thus for a 40 cm RLG we have

$$\phi_{\min} = (0.5-1.0) \times 10^{-3} \text{ rad.} \quad (\text{III-2})$$

One can achieve a phase shift  $\phi$  of this magnitude using a pure Fe thin film mirror operating in the transverse Kerr mode. If we use Eqs. IV-1 and IV-4 of Report No. 1 together with the N and Q values of Fe given there we find that  $\phi(\text{Fe}) = 0.99 \times 10^{-3} \text{ rad}$  for  $\lambda = 6328 \text{ \AA}$  and an angle of incidence  $\phi$  of  $30^\circ$ . However, the p-polarized reflectivity of such a bare film is only 0.505. It is impossible to tolerate such high losses in a RLG where high quality multilayer dielectric (MLD) mirrors have reflectivities in excess of 0.999. Low reflectivities are characteristic of all the transition metal alloys which might be used for such mirrors and hence one must use MLD stacks on top of the magnetic alloy films to achieve a high reflectivity. We now discuss how to evaluate the phase shift and loss in such an MLD-magnetic mirror element and restrict the discussion of the transverse Kerr effect for simplicity.

#### A. Magnetic Mirror Overlaid with a Dielectric Stack

We consider a p-polarized wave  $E_0$  incident on a metallic magnetic mirror overlaid with a dielectric stack to improve the reflectivity, as illustrated in Fig. 3.

The electric field of the reflected component consists of three parts

$$E_R = E_d + E_m + E_M \quad (\text{III-3})$$

where  $E_d$  is reflected from the dielectric stack,  $E_m$  is the reflected field from the metallic mirror as modified by the stack, and  $E_M$  is that reflected field from the mirror due to its magnetization.

The dielectric mirror is represented by a complex reflection coefficient  $r_d$  and transmission coefficient  $t_d$ . The distance between the last interface of the stack and the mirror is  $z$  while the intervening material has a real propagation constant  $\beta$  (i.e. there is no loss). The Fresnel coefficient  $r_p$  at the mirror interface is given (Report No. 1 (IV-1)) by

$$r_p = r_p^0 (1 + AQ). \quad (\text{III-4})$$

Hence we have

$$E_d = r_d E_0$$

$$\begin{aligned} E_m &= t_d Z_\ell r_p^0 Z_\ell t_d E_0 \\ &= e^{-2i\beta\ell} t_d^2 r_p^0 E_0 = r_m E_0 \end{aligned}$$

$$E_M = e^{-2i\beta\ell} t_d^2 r_p^0 AQ E_0 = r_M E_0$$

where  $Z_\ell = e^{-i\beta\ell}$  is the propagation factor.

Thus  $E_R = (r_d + r_m + r_M) E_0$ . And for reasonable parameter values we expect

$$|r_d| \gg |r_m| \gg |r_M|.$$

#### B. Optimum Construction

We wish to adjust  $E_M$  so that we get the maximum magnetically induced phase shift in  $E_R$ . This will clearly be true if  $r_M$  is  $90^\circ$  out of phase with  $r_d$ , i.e.  $\text{Re}(r_M/r_d) = 0$ . We do this by adjusting the length  $\ell$  which is a free parameter. Upon reversal of the magnetization (and  $Q$ ) the induced phase shift is (with such a maximization)

$$\begin{aligned} \phi &= 2 \text{Im}(r_M/r_d) \\ &= 2 |r_M/r_d| \end{aligned} \quad (\text{III-5})$$

$$\begin{aligned} \text{Now } |r_M| &= |t_d|^2 |r_p^0 AQ| \\ &= (1-R_d) |r_p^0| |AQ| \end{aligned}$$

where  $R_d$  is the reflectivity of the dielectric stack alone so that  $(1-R_d) = L_d$ , the stack loss (transmission).

So we get

$$\phi = 2L_d |r_p^0/r_d| |AQ| \quad (\text{III-6})$$

and a reasonable figure of merit is

$$\text{FM} = \phi/L_d = 2|r_p^0AQ/r_d| \quad (\text{III-7})$$

We note the following:

- 1) One can tune the stack-mirror combination to maximize  $\phi$ .
- 2) This same setting eliminates the magnetically induced intensity variations because  $\text{Re}(r_M/r_d) = 0$ .
- 3)  $\phi$  is proportional to  $L_d$ .
- 4) To maximize the figure-of-merit one maximizes
  - a)  $|Q|$  and
  - b)  $|r_p^0| = \sin 2\phi_i |(N/n_a)\cos\phi_i + \gamma|^{-2}$ .
- 5) One wants to use the material with the highest  $|Q|$ .
- 6) One wants to use a material with a large  $n_a$  adjacent to the magnetic mirror.

Let  $\phi_{\min}$  be the minimum acceptable phase shift for a RLG. Then one can calculate the minimum mirror losses from Eq. (III-6).

$$L_d^{\min} = \phi_{\min}/2 |r_p^0AQ/r_d|$$

If the laser transition has a gain per unit length of  $G$ , then the minimum length for the laser is given by

$$(1-L_d)(1-G\ell_{\min}) = 1$$

The above analyses gives an oversimplified view of the phase shift maximization process because it neglects the field component  $E_m$  as well as the possibility of multiple reflections in the dielectric layer next to the metal mirror. However, since  $|r_m| \ll |r_d|$ , the results are a reasonable approximation of the real situation.

(In order to treat multilayer dielectric-magnetic film devices in a fully quantitative fashion, we have developed a computer program based on the work of Hunt.<sup>5</sup> The structure and capabilities of this program will be spelled out in a forthcoming report. However, some of the numerical results for the figure of merit of dielectric stack overcoated metallic magnetic mirrors will be quoted in the present report.)

For definiteness, let us consider such a mirror based on Fe at  $\lambda = 6328\text{\AA}$ . To enhance  $|Ar_p^0|$  we take the layer adjacent to the opaque Fe film to have a large index of refraction, e.g.  $n_a = 2.36$  (ZnS). Then for a  $30^\circ$  external angle of incidence the internal angle  $\phi_i = 12.3^\circ = \sin^{-1}(\sin 30^\circ / 2.36)$ . The Q and N values of Fe are taken from Report No. 1 and yield  $|Q| = 0.034$  and  $|Ar_p^0| = 0.065$ . Approximating  $|r_d| = 1$  one gets

$$L_d^{\min} = 226 \phi_{\min}(\text{rad}).$$

Thus if we take  $\phi_{\min} = 5 \times 10^{-4} \text{ rad}$  (see III-2), we obtain  $L_d^{\min} = 0.113 = 11.3\%$  loss. This is an unacceptably large optical loss. (An improved calculation using the computer program just mentioned gives 8.2% loss for the mirror. This loss is still excessive.) At  $\lambda = 6328\text{\AA}$  it is not possible to improve significantly on this situation for a transverse Kerr mirror with any of the materials examined in Report No. 1.

### C. Figure-of-Merit

The figure-of-merit as defined in Eq. (III-7) is dependent on the angle of incidence  $\phi$ . It would be better to have no such dependence. One can do this by using a fixed external angle (e.g.  $\phi = 30^\circ$ ) or separating out the angular dependence. The latter approach is used here.

Assume the dielectric loss  $L_d$  is small so that  $|r_d| \approx 1$ . Then expand Eq. (III-7) to obtain

$$\phi = 2L_d |Q| \cdot |(N/n_a) \cos \phi_i + \delta|^{-2} \sin 2\phi_i \quad (\text{III-8})$$

where the internal angle of incidence  $\phi_i$  at the metal film is given by

$$n_a \sin \phi_i = \sin \phi$$

Hence  $\cos \phi_i = [1 - n_a^{-2} \sin^2 \phi]^{1/2}$ . Also to increase  $\phi$  one wants  $n_a$  as large as possible. Assume that  $n_a \geq 2$  and  $\phi \leq 60^\circ$  for a reasonable RLG. Then  $1 \leq \cos \phi_i \leq 0.90$ , so we can approximate  $\cos \phi_i$  by 1. Also  $\gamma = [1 - N^{-2} \sin^2 \phi]^{1/2}$  is even better approximated by 1. Thus Eq. (III-8) becomes

$$\phi = 4L_d |Q| \cdot |N + n_a|^{-2} n_a \sin \phi \quad (\text{III-9})$$

Hence an angularly independent transverse Kerr figure-of-merit can be defined as

$$(\text{FM})_T \equiv |Q| n_a |N + n_a|^{-2} \quad (\text{III-10})$$

This definition is used in this report.

We note that

$$|N + n_a|^2 = (n + n_a)^2 + k^2.$$

Let

$$z \equiv n_a |N + n_a|^{-2} = n_a \{ (n + n_a)^2 + k^2 \}^{-1}$$

$$\begin{aligned} \frac{dz}{dn_a} &= \{ \}^{-1} - 2n_a (n + n_a) \{ \}^{-2} \\ &= [n^2 + 2nn_a + n_a^2 + k^2 - 2nn_a - 2n_a^2] \{ \}^{-2} \\ &= (n^2 + k^2 - n_a^2) \{ \}^{-2} \\ &= 0 \text{ for } n_a^2 = n^2 + k^2. \end{aligned}$$

Thus  $(FM)_T$  is maximum for  $n_a^2 = n^2 + k^2$ .

#### IV. PROPERTIES OF METALLIC MAGNETIC MATERIALS

The present study concerns itself with binary alloys of transition metals and rare-earths which appeared to be promising candidates for exhibiting useful magneto-optic effects. These alloys tend to form two-sublattice ferrimagnetic systems in which the rare-earth moments composing one sublattice tend to oppose the transition metal moments composing the other sublattice. At a particular composition, called the compensation composition, these two sublattice moments just cancel, leaving a net magnetic moment of zero for the complete system. In the vicinity of this compensation composition, the anisotropic magnetic properties of the rare-earths play an extremely useful role in creating magnetic films which possess permanent magnetic moments normal to the film plane. Such films might form the basis of a polar Kerr effect mirror as employed in a four-frequency (or multi-oscillator) laser gyro.

The optical and magneto-optical properties of these alloy systems were not available in the open literature, therefore several representative series of alloys were prepared and characterized. The samples were prepared by e-beam evaporation as discussed in Report No. 1. The two rare-earths, Gd and Tb, are low and high anisotropy ions respectively. They were chosen to establish the dependence of the optical properties upon anisotropy. They were alloyed with the two transition metals which show the largest magneto-optic effects, Fe and Co. The optical constants  $n$  and  $k$ , as well as the magneto-optical constants  $Q_1$  and  $Q_2$ , were determined using the techniques described in Report No. 1 and the analysis in Section II of this Report. In addition, the magnetization as a function of applied field was measured for all the samples using standard techniques.

##### A. Optical Properties

###### 1. Alloys of Rare-Earths and Transition Metals

The values of  $n$  and  $k$  for the series of alloys and pure elemental samples studied are given in the first two columns of Table I for  $\lambda = 0.63\mu\text{m}$ . It should be noted that  $2.2 < n < 3.2$  and  $2.8 < k < 3.9$  for all of the samples measured, and only slight systematic variation of either  $n$  or  $k$  with composition is seen (Table 1). For this reason, representative calculations can often be carried out using

the optical constants of Fe ( $n=2.75$ ,  $k=3.23$ ).

The magneto-optical constants have a much more interesting dependence upon composition. The values of  $Q_1$  and  $Q_2$  are given in the third and fourth columns of Table I and exhibited graphically in Figs. 4 and 5. The most important feature of Fig. 4 is that in every case the compositional variation causes  $Q_1$  to change sign as

the transition metal (Fe or Co) is diluted by a rare-earth (Gd or Tb). This change of sign occurs in the area of the compensation composition (75% to 85% transition metal). It is just at this composition that the roles of the two sublattices reverse. When the transition metal concentration is above that at compensation, it is the dominant sublattice (possessing the larger magnetic moment) and it aligns with the applied field. When one passes through compensation, the rare-earth sublattice assumes the larger magnetic moment. Since the two sublattices are locked in opposition by the exchange forces between them, when the rare-earth sublattice reverses to align with the field, the transition-metal sublattice is also forced to reverse and now is directed against the applied field. Since  $Q_1$  is a maximum for the pure transition metals and decreases with the addition of rare-earths, it appears as if  $Q_1$  arises primarily from the transition metal sublattice and changes sign when the latter reverses.  $Q_2$ , on the other hand, was a negative quantity for almost all compositions. As can be seen in Fig. 5, for the Co-based alloys,  $Q_2$  tends toward zero almost monotonically with increasing rare-earth content. For Fe:Gd there may be a maximum in  $Q_2$  near the compensation composition, but the Fe:Tb alloys showed no systematic behavior. It should be noted that the behavior of both  $Q_1$  and  $Q_2$  for the Co-based alloys was essentially independent of the rare-earth used (i.e. Gd or Tb) although these two elements are magnetically quite dissimilar. The magnetic properties of Gd arising from electron spin, while those of Tb arise to a great extent from electron orbital momentum. The Fe-based alloys seem to distinguish between Gd and Tb, but the compositional dependence of  $Q_1$  and  $Q_2$  in the Fe:Tb alloys did not exhibit a smooth variation. This may reflect a tendency toward a formation of several possible stable crystal phases characteristic of the Fe:Tb system and the simple ratio of Fe:Tb during film growth may not represent the actual composition of the portion of film sampled by the laser beam during measurement.

For many magneto-optical applications  $|Q|$  is in fact the most useful parameter for measuring performance. This was shown earlier to be true for the Figure-of-Merit of the ring laser gyro. Therefore  $|Q|$  is presented in Fig. 6 again as a function of rare-earth content in these Fe and Co-based alloys. In every case addition of the rare-earths caused a decrease in  $|Q|$ . This decrease was more severe in the Co alloys, and aside from pure Fe itself, the highest  $|Q|$  was obtained with nominally 30% to 40% Tb in Fe.

The final question of interest regarding the magneto-optical properties concerns the dependence of  $|Q|$  upon the saturation magnetization  $M_s$ . In simple ferromagnetic materials it is found that  $|Q|$  is proportional to  $M_s$ . For example, in the previous report<sup>1</sup> in which Fe was alloyed with various non-magnetic metalloids (e.g. Si or B), the dilution of the Fe caused a decrease in both  $|Q|$  and  $M_s$ , but the ratio  $|Q|/M_s \approx 20 \times 10^{-6} \text{ G}^{-1}$  was obtained for all such alloys independent of either the metalloid or its content. The same value of this ratio was found for Ni, Co and permalloy as well. In Fig. 7, however, we see that this is not the case for these two-component ferrimagnets. The value of  $|Q|/M_s$  reaches a maximum for all of these materials in the vicinity of their compensation compositions. While there are not enough data points to locate these values precisely, it is clear that  $|Q|$  does not go to zero where  $M_s$  does. This result confirms our earlier observations concerning  $Q_1$ , namely that the magneto-optical properties do not depend upon the total magnetization  $M_s$ , but rather upon the magnetization of the transition-metal sublattice. That is, while the rare earths contribute to the total magnetic moment of these alloys, the magneto-optical properties arise largely from the magnetization of the transition metal moments. This is an important result for guiding future work on materials of these types.

## 2. Selected Materials at $\lambda = 1.15\mu\text{m}$

Also included in this report is the determination of  $n$ ,  $k$ ,  $Q_1$ ,  $Q_2$  at  $\lambda = 1.15\mu\text{m}$  for the most important soft magnetic materials discussed in the previous report, where only  $\lambda = 0.63\mu\text{m}$  data was included. This additional data has been obtained because of the interest within the ring laser gyro community in using this alternative He-Ne laser

transition. In every case the very same samples were measured so that meaningful comparisons could be made between these two reports. The samples were stored in a vacuum dessicator between measurements and all data was taken at the glass/metal interface to avoid surface effects. The measurement techniques employed are essentially the same as described earlier in this report, and in the previous report, except for changes in the source and detector. A He-Ne laser operated at  $\lambda = 1.15\mu\text{m}$  was substituted for the  $\lambda = 0.63\mu\text{m}$  He-Ne laser previously used, and a InSb photovoltaic detector operating at  $77^\circ\text{K}$  replaced the Si photo-diode. Since the prism coupling procedure (described in Report No. 1) is independent of any dispersive properties of the fused quartz prism, the  $70^\circ$  angle of incidence geometry was employed for  $\lambda = 1.15\mu\text{m}$  just as it was for  $\lambda = 0.63\mu\text{m}$ . Certain straight-forward alignment procedures were adopted which enabled one to completely align the sample using a  $\lambda = 0.63\mu\text{m}$  He-Ne laser and then substitute a coaxial  $\lambda = 1.15\mu\text{m}$  He-Ne laser beam using kinetic optical mounts.

The values obtained for  $n$ ,  $k$ ,  $Q_1$ , and  $Q_2$  are given in Table II. for these selected samples at  $\lambda = 0.63\mu\text{m}$  and  $\lambda = 1.15\mu\text{m}$ . While it can be observed that both  $n$  and  $k$  increase for all samples as one goes to the longer wavelength, the most important feature is the dramatic increase in  $|Q|$ . This arises largely from an increase in  $Q_2$ . The relation of these results to the use of these materials in a magneto-optic biasing element will be discussed in the following section.

### B. Figure-of-Merit

In this report a new expression for the figure-of-merit  $(\text{FM})_{\text{T}}$  of a transverse Kerr mirror is obtained in Section III, Eq. (III-9). It is believed that this is a more useful definition than that proposed in the previous report in that it reflects the behavior of the magneto-optic metal when it is incorporated in a realistic mirror structure. Using this new definition, the  $(\text{FM})_{\text{T}}$  of the materials presented in the previous report has been recalculated from their fundamental physical properties and is presented here in Fig. 8. The mirror structure assumes that the adjacent layer is ZnS ( $n_a = 2.36$  at  $\lambda = 0.63\mu\text{m}$ ).

The results shown in Fig. 8 do not exhibit the anomalous features generated by the previous definition of  $(\text{FM})_{\text{T}}$  in Fig. 13 of Report No. 1. There is now a smooth composi-

tional dependence of the Fe-B series, and the Fe-Ni series can be seen to easily extrapolate to pure Fe. The clustering of the Fe-Si alloys is believed to be connected by their tendency toward crystallinity and the formation of few stable phases, as contrasted with the Fe-B series which forms a continuous series of amorphous alloys. The high performance of the Fe/Fe-Ni "sandwich" samples, while real, should be judged with the same caveats raised in the previous report.

It is useful to compare these results for the calculation of  $(FM)_T$  with those obtained using the computer model referred to earlier in this report. The same mirror structure is modeled, namely a dielectric stack with a tuning layer over the metal film. The principal difference between the two calculations is that multiple reflections within the tuning layer are ignored by the approximate calculation used in this report. Because of this, the computer model yields much sharper "resonance" behavior when the tuning layer thickness is varied and somewhat higher peak values for  $(FM)_T$ . In order to compare the values obtained from these two calculations a graph was prepared, as shown in Fig. 9 which plots  $(\Delta\phi/\text{Loss})_{\text{max}}$  versus  $2(FM)_T$ , where  $\Delta\phi$  and  $(\text{Loss})$  are the computer calculated values for the differential phase shift and total optical loss for the mirror structure operated at  $30^\circ$  angle of incidence, while  $2(FM)_T$  is  $\Delta\phi/\text{loss}$  from Eqs. (III-8 and III-9) using the same angle. If Eq. (III-9) were exact, one would expect all of the points to fall on a straight line with a slope of 1.0. While there is some scatter, the most striking result is that the data for most materials do fall approximately on a straight line at a given wavelength. This implies that there is a reasonably consistent relationship between the two calculations, and that ranking of materials in order of performance may indeed be done using the much simpler approximate formula with reasonable confidence.

In addition to confirming the usefulness of Eq. (III-9) for  $(FM)_T$ , Fig. 9 also illustrates that of all the materials measured, only Fe showed a significant improvement in performance at the longer wavelength (approximately 50%). The slope of the line is 1.42 at  $\lambda = 0.63\mu\text{m}$  and is 1.84 at  $\lambda = 1.15\mu\text{m}$ . This means, of course, that the values given by the approximate formula are uniformly less accurate as one goes to longer wavelengths. This is probably due to the increase in optical index contributing to the multiple reflections mentioned above.

### C. Magnetic Properties

The magnetic properties of interest in these materials, besides the magneto-optic properties already discussed, all have to do with the magnetization vector  $\vec{M}$ . It is important to know its dependence upon applied magnetic fields, and its directional properties. These two phenomena are generally interconnected through the property of magnetic anisotropy, that is, the response to an applied magnetic field depends upon the direction in which it is applied to the magnetic film. There are forces created within the film during growth which tend to direct the magnetization to lie in a preferred direction. In addition, there is the classical "demagnetizing force" created by magnetic poles on a surface which opposes the orientation of  $\vec{M}$  perpendicular to a plane, favoring instead  $\vec{M}$  lying in the plane. The demagnetizing force is proportional to the total magnetization of the material. In two-sublattice ferrimagnets near the compensation composition, where  $\vec{M}$  approaches zero the demagnetization force disappears and the orientation of  $\vec{M}$  depends only upon applied field and growth anisotropies. The preferred direction for the magnetization is called the "easy" axis i.e., the sample is easily magnetized along this direction in relatively low applied fields or, in the case of a permanently magnetized sample,  $\vec{M}$  lies in this direction. Directions orthogonal to this axis are called the "hard" axes. In planar samples, such as the ones discussed in this program, it is possible to have an "easy" plane, i.e.,  $\vec{M}$  is equally free to lie anywhere in the plane, the "hard" axis being normal to the plane. If there is some anisotropy in the plane, which often occurs in binary alloys during film fabrication, then an additional axis may be generated within the plane. That is there may be an "easy" and "hard" axis in the plane, and an additional, even harder axis normal to the plane. Such cases are common when binary alloys are prepared by vacuum evaporation from separate sources and they arise from the geometry of the evaporation configuration. There is an even more complicated case in which the "easy" axis lies neither in the plane nor normal to it, but rather at some skew angle to the surface. This can result from the competition between growth induced anisotropy and the demagnetizing force.

These remarks on the orientation of  $\vec{M}$  must be kept in mind when considering the applications of magnetic thin films for a specific purpose. For example, in Report No. 1 the binary alloys of Fe with the metalloids B and Si all possessed an easy axis in the plane of the film and data were provided for the field dependence of  $\vec{M}$  along that

axis. The occurrence of easy axis in that case was useful since the intended application was for transverse Kerr effect mirrors. An easy axis in the plane facilitated fast switching while providing immunity to either stray magnetic fields or irregularities in the applied switching field.

On the other hand, in a multi-oscillator gyro design a permanently magnetized magneto-optic biasing element is employed. One generally wishes to operate with nearly circular polarization and the polar Kerr effect is utilized with the magnetization normal to the surface. This can only be achieved by the introduction of some anisotropy as discussed above. Crystalline materials can often be grown to exhibit this anisotropy as a result of their crystal structure. In the case of amorphous ferrimagnetic materials, such as the alloy systems discussed in this report, growth anisotropies must be utilized. As discussed above, they tend to become dominant only in the vicinity of the compensation composition. These considerations led to the investigation of these ferrimagnetic systems.

A detailed understanding of the orientation of  $\vec{M}$  in these alloys would require a magnetization "mapping" of each sample, i.e., one would have to measure the component of  $\vec{M}$  normal to the plane, as well as the components along two axes in the plane, as a function of applied magnetic field. Such a time-consuming effort, while of interest from a basic research point of view, is not justified in a survey study as is being carried out here. The principal concern for the magneto-optic applications is whether there is a component normal to the surface in the absence of an applied field and what is its magnitude.

This can be determined in two ways. First, from the measurements of the normal components of the magnetization. These results are presented in Table III. One can also see this same result directly from the ellipsometric measurements of the polar Kerr effect. These results are presented in detail in Figs. 10 through 17. The axis of these figures is centered on the values obtained from an aluminum mirror used as reference. The polar Kerr effect measurements were carried out in the configuration illustrated in Fig. 2, and, as shown earlier, from the analyzer measurements one obtains the Kerr rotation, while from the polarizer settings one obtains the induced ellipticity. The data in Figs. 10 through 17 were obtained only at  $H = +22, 0, -22, 0$  kOe respectively and the points were connected by straight lines merely to guide the eye. The shape of a true hysteresis curve between these points may be different.

Inspection of these Figures yields several interesting pieces of information. Most striking is the fact that while the "hysteresis" curves for the pure metals Ni, Fe, and Co (Figs. 10 and 11) are to within experimental uncertainty centered on the origin, many of the curves of the alloys are not. In the case of the ellipticity this indicates that in the absence of an applied field, either the sample itself possesses linear birefringence and acts as a waveplate, or exhibits differential reflectivity for opposite circular polarizations. Furthermore, the ellipticity depends upon applied field. In the case of the rotation, there is a similar indication that even in the absence of an applied field one obtains rotation and depending upon the direction of the applied field it can be either increased or decreased.

All of these observations are consistent with a picture discussed earlier in this Section, namely that the easy axis of magnetization lies at some skew angle out of the surface. The applied field normal to the surface tends to pull the moment away from this zero field angle altering the magnitude of the component normal to the surface, hence changing both the measured ellipticity and rotation. Those curves which are hysteretic (i.e. open) indicate that when sufficiently high fields are applied in an opposing direction, the magnetic moment does not return to its original angle. Some curves show a "flat" behavior for a given applied field direction indicating either that the moment is already nearly normal to the plane in zero field, or that very strong anisotropy forces oppose its motion in that direction. One even sees (e.g. Fig. 12, curve C) in some samples a decrease of ellipticity with applied field.

This peculiar result can also be seen to stem from the two-sublattice ferrimagnetic structure of these materials. As discussed above, the total magnetic moment is the sum of the moments of the two-sublattices, which are in general opposed, but may not necessarily be co-linear, as illustrated in Fig. 18. When an external magnetic field is applied normal to such a film, internal exchange forces would tend to keep the relationship between these magnetization vectors fixed while  $\vec{M}_T$  aligns itself with the field. Clearly the projection of either  $\vec{M}_1$  or  $\vec{M}_2$  along a normal to the surface may decrease. Since we now know that the magneto-optic behavior is principally caused by only the transition-metal sublattice, one can readily see how its contribution to a polar Kerr effect can decrease as the applied field is increased. It should be noted that

Fig. 18 is meant merely to illustrate one possible model. The exact sublattice behavior in these alloys has not yet been determined.

## V. Conclusions

In this report we have provided a thorough description of the ellipsometric measurement procedures used to obtain the magneto-optic data, an improved definition of the Figure-of-Merit for the practical application of materials as magneto-optic bias elements in ring laser gyros, and the characterization of some new magneto-optic materials.

The first item does not need any further discussion. The second item prompted the construction of a mathematical model, which is capable of describing the performance of practical magneto-optic biasing elements. This model has been cast into computer language and a detailed description as well as many applied results will be provided in the next Report of this series. The third item provides a considerable amount of new information which deserves to be commented upon.

### A. Performance at 1.15 $\mu\text{m}$ vs. 0.63 $\mu\text{m}$

The improvement in the Figure-of-Merit of Fe at  $\lambda = 1.15\mu\text{m}$  as compared with  $\lambda = 0.63\mu\text{m}$  can be attributed to the fact that the optical properties depend upon two physical mechanisms, the conduction electrons and the more localized electrons bound to the atoms. The oscillator strengths of these bound electrons have a spectral dependence consisting of distinct resonances. One of the principal resonances occurs in the vicinity of  $1.0\mu\text{m}$ .<sup>7</sup> In this region there is a considerable contribution to  $Q_2$ , while the contribution to  $Q_1$  changes little. This can be seen from the measured values in Table II. There is a similar increase in  $Q_2$  for Co for similar reasons, while in Ni, where there is no such resonance,  $Q_2$  changes little. The Fe-alloys measured show more complicated behavior. Alloying with metalloids (B and Si) gives the same enhanced  $Q_2$  as in pure Fe, but the contribution to  $Q_1$  is decreased. The high Ni alloys, of course, are more characteristic of Ni than of Fe. One can see from this that it is clear why pure Fe mirror surfaces performed better at  $1.15\mu\text{m}$  than they do at  $0.63\mu\text{m}$ , and why laser gyros based upon such a mirror may operate successfully only at the longer wavelength. One should also be careful to note that not all

materials allow one to extrapolate to longer wavelength and expect better performance.

### B. Alloys of Rare-Earths and Transition Metals

Discussion of the two-sublattice ferrimagnets is not as straightforward as the above alloy systems. It is clear that one can exploit the compensation phenomenon and the magnetic anisotropies to produce mirrors which will have a permanent magnetic moment out of the mirror plane. The samples studied here did not in general have moments normal to the plane because of the geometry employed during evaporation. This problem can be overcome either by sputtering a homogeneous material or by rotating the substrate during evaporation.<sup>6</sup> Either technique averages the canted angle of the magnetization about the normal to give only a resultant perpendicular component.

From the data of Table III, in particular the compositional dependence of the Co-Tb alloys, one sees that in the vicinity of compensation one obtains very large coercive fields ( $H_C$ ). These are the applied magnetic fields required to reduce the magnetization to zero. Note also that in this region, the saturation magnetization ( $M_S$ ) is approximately equal to the remanent magnetization ( $M_R$ ). These properties imply a flat-topped hysteresis curve and a material which is very insensitive to external fields. For compositions away from compensation  $H_C$  decreases,  $M_S$  becomes greater than  $M_R$  and the resulting hysteresis curve loses its squareness. This is the "classic" behavior of these two-sublattice ferrimagnets' dependence upon composition. In the other alloy systems listed in Table III, the data is not always complete enough to illustrate this pattern as well, but the trends are the same. Choosing the composition on the basis of the largest normal moment is not sufficient. Since the magneto-optical effects arise principally from the transition-metal sublattice, one should choose a composition on the transition-metal-rich side of compensation. In this region of composition the material can be optimized by choosing the maximum amount of transition metal still compatible with a net moment normal to the plane.

### C. Recommendations

From a magneto-optical point of view, the best performance is obtained from the Fe-based alloys. Further work

on Co:rare-earth alloys does not appear to be indicated. Careful preparation of Fe-Tb alloys near compensation seems promising, since Fe<sub>.70</sub>Tb<sub>.30</sub> has  $|Q|$  of approximately 75% of pure Fe. Preparation techniques should avoid crystalline formation which results in an undesirable separation of phases. Furthermore, the good performance of Tb, which is highly anisotropic, suggests that the two other high-moment high anisotropy rare-earth ions Ho and Dy should be considered as potentially useful alloys with Fe near the compensation composition.

#### References

1. "Magneto-Optic Materials for Biasing Ring Laser Gyros - Report No. 1", J.J. Krebs, G.A. Prinz, D.W. Forester, and W.G. Maisch, NRL Memorandum Report 3870, April 1978.
2. "Manual on Ellipsometry", R.J. Archer, 1968, available from Gaertner Scientific Corp., Chicago, IL.
3. "Ellipsometric Measurement of the Kerr Magneto-Optic Effect", H.T. Minden, Applied Optics 18, 813 (1979).
4. "A Survey of Magneto-Optic Effects", M.J. Freiser, IEEE Trans. Magnetics MAG-4, 152 (1968).
5. "Magneto-Optic Scattering from Thin Solid Films", J. Appl. Phys. 38, 1652 (1967).
6. "Physical Vapor Deposition", Airco Temescal (1976), p. 83, available from Airco Temescal, 2850 Seventh Street, Berkeley, CA 94710.
7. "Magneto-Optical Properties of Ni, Co, and Fe in the Ultraviolet Visible and Infrared Parts of the Spectrum", G.S. Krinchik and V.A. Artem'ev, Zh.Eksp.Teor.Fiz. 53, 1901-1912 (December, 1967), reprinted in Soviet Physics JETP 26, 1080 (1968).

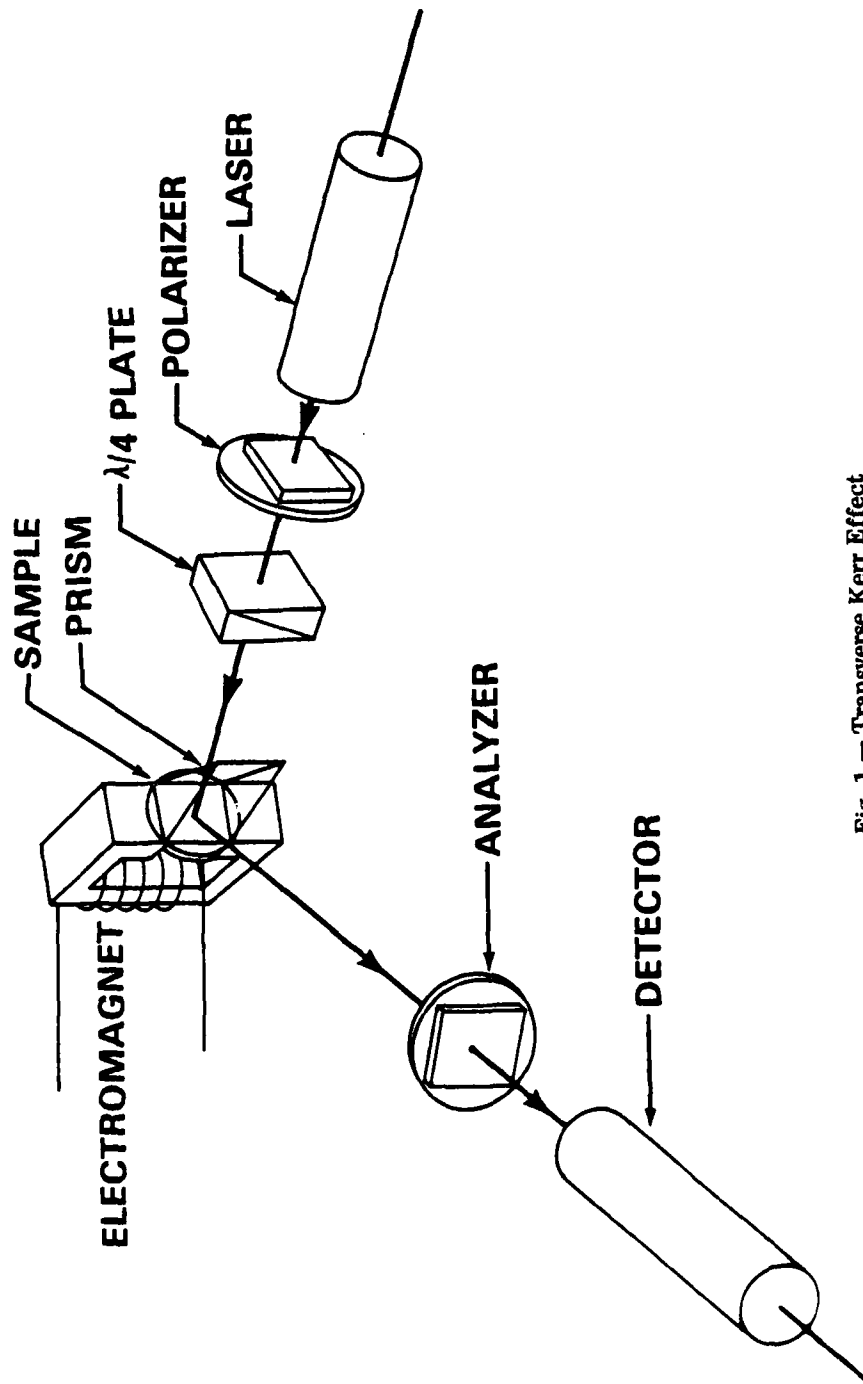


Fig. 1 — Transverse Kerr Effect

POLAR KERR EFFECT

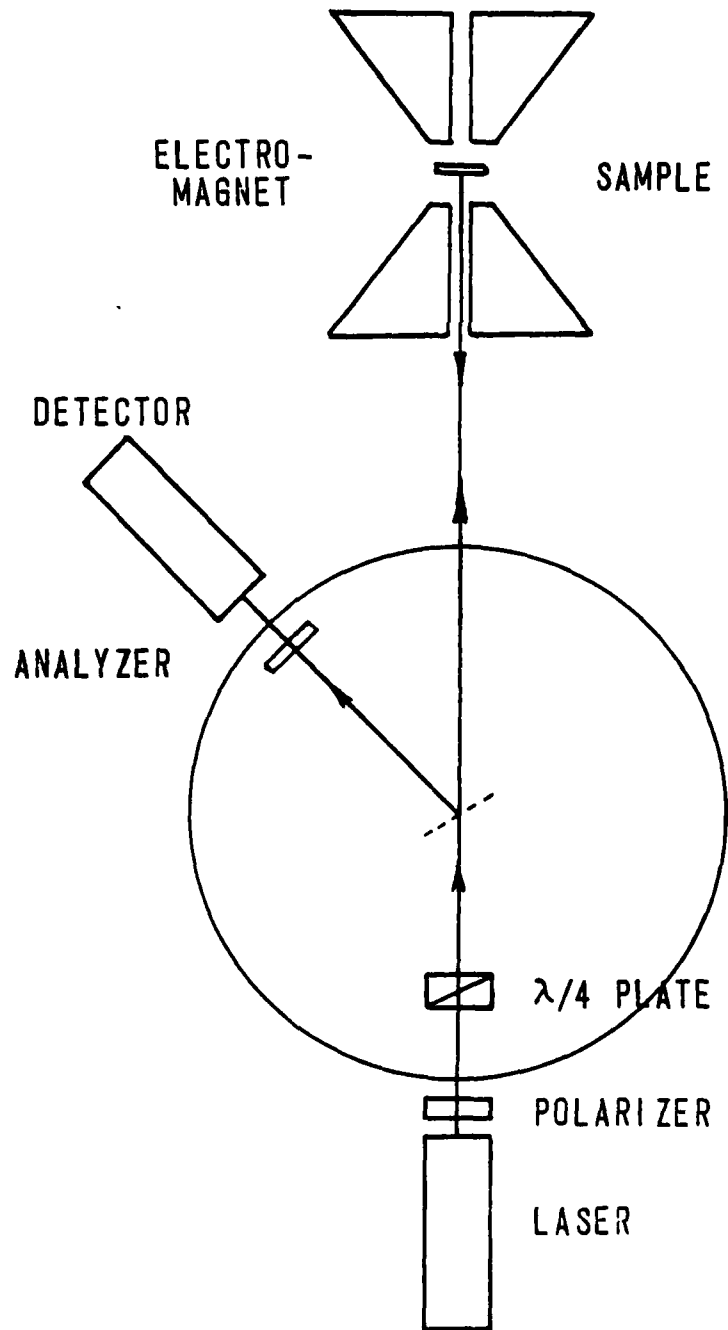


Figure 2

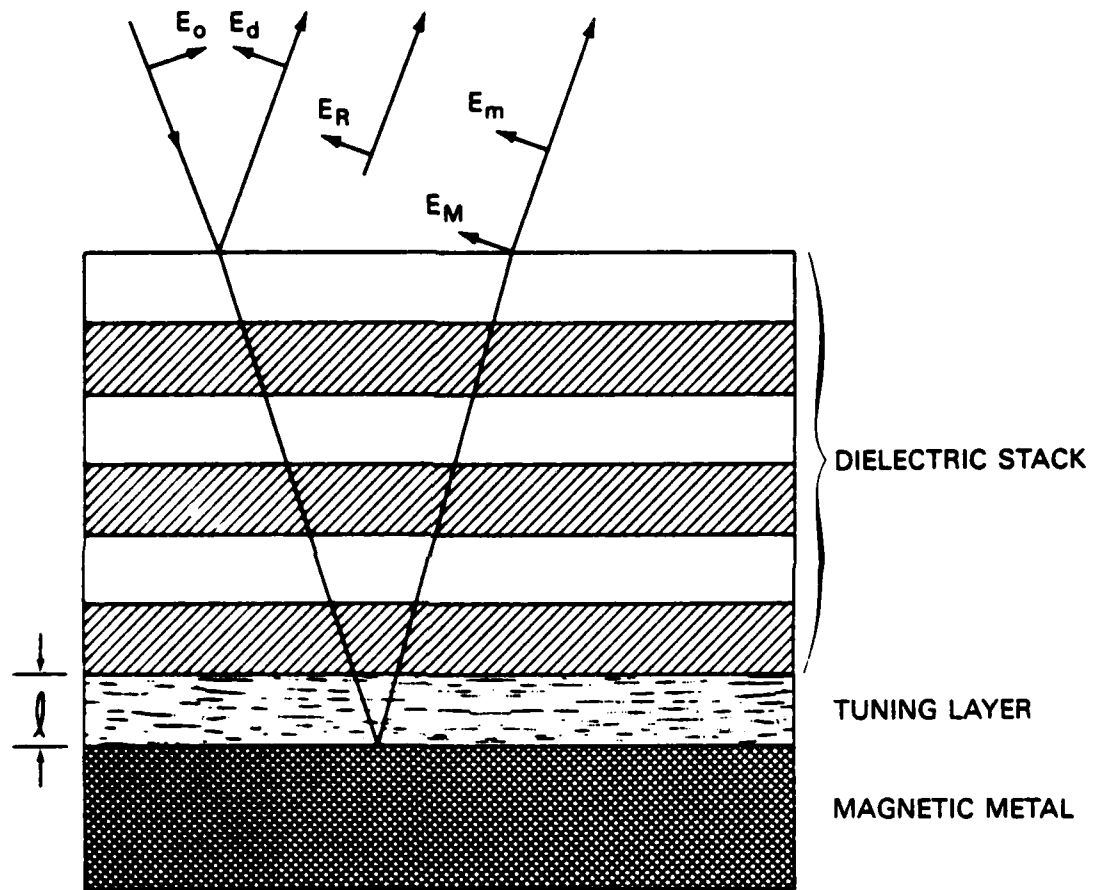


Figure 3

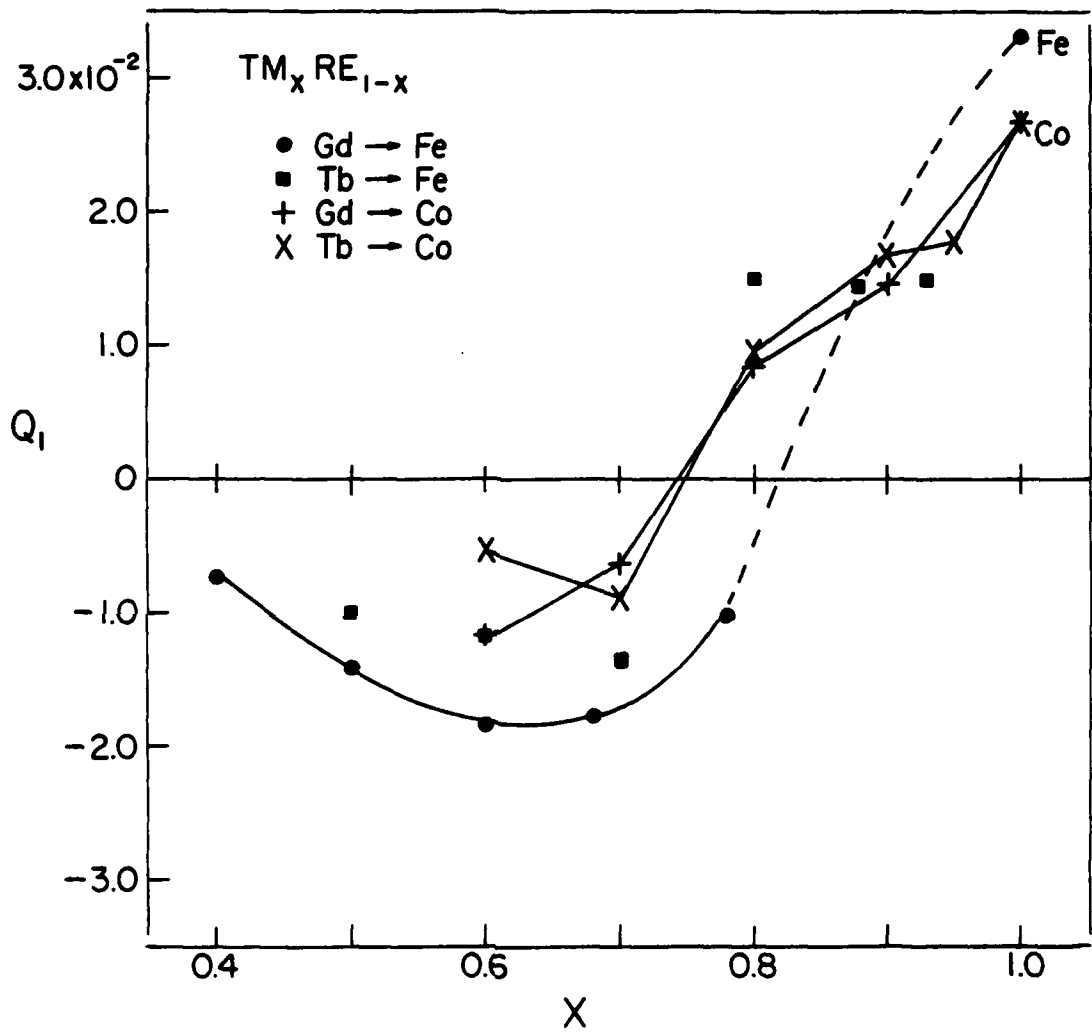


Figure 4

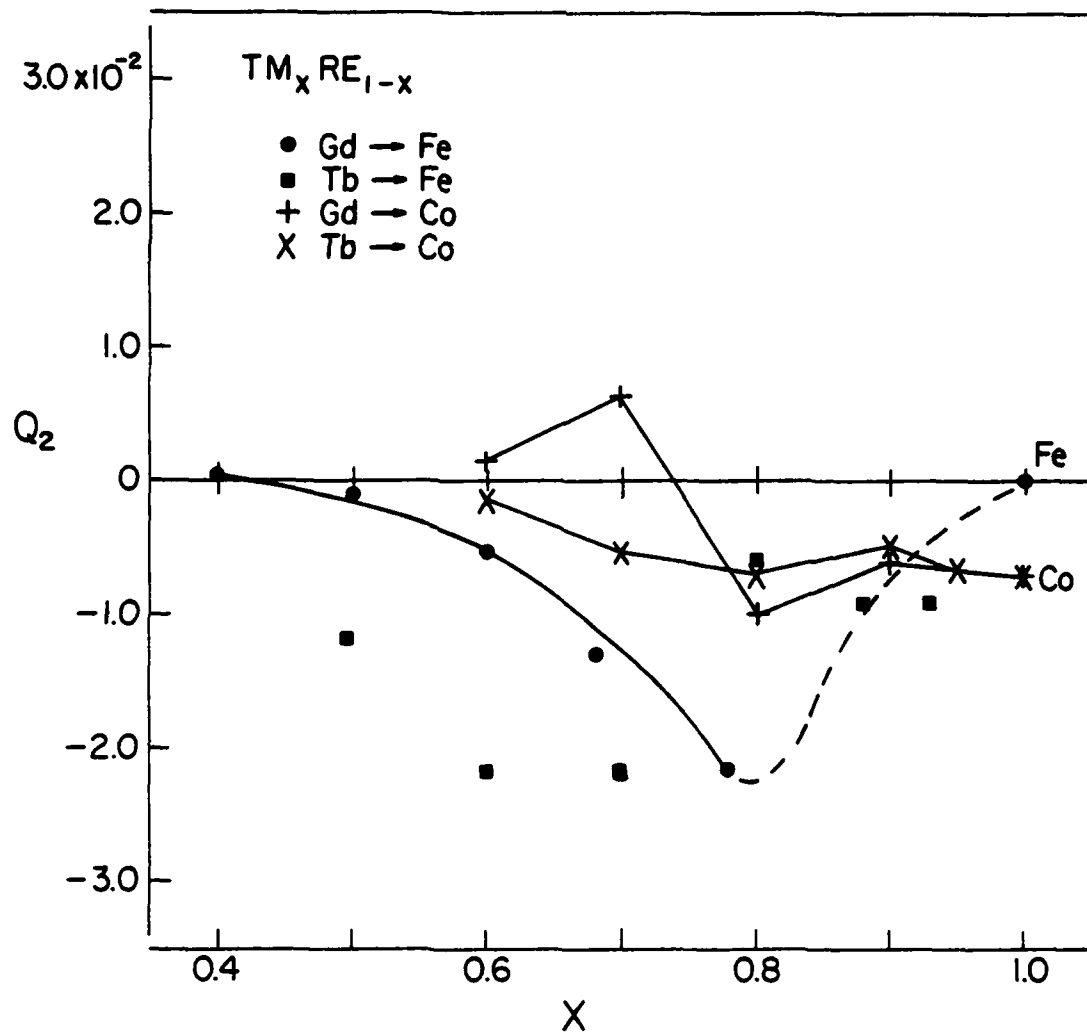


Figure 5

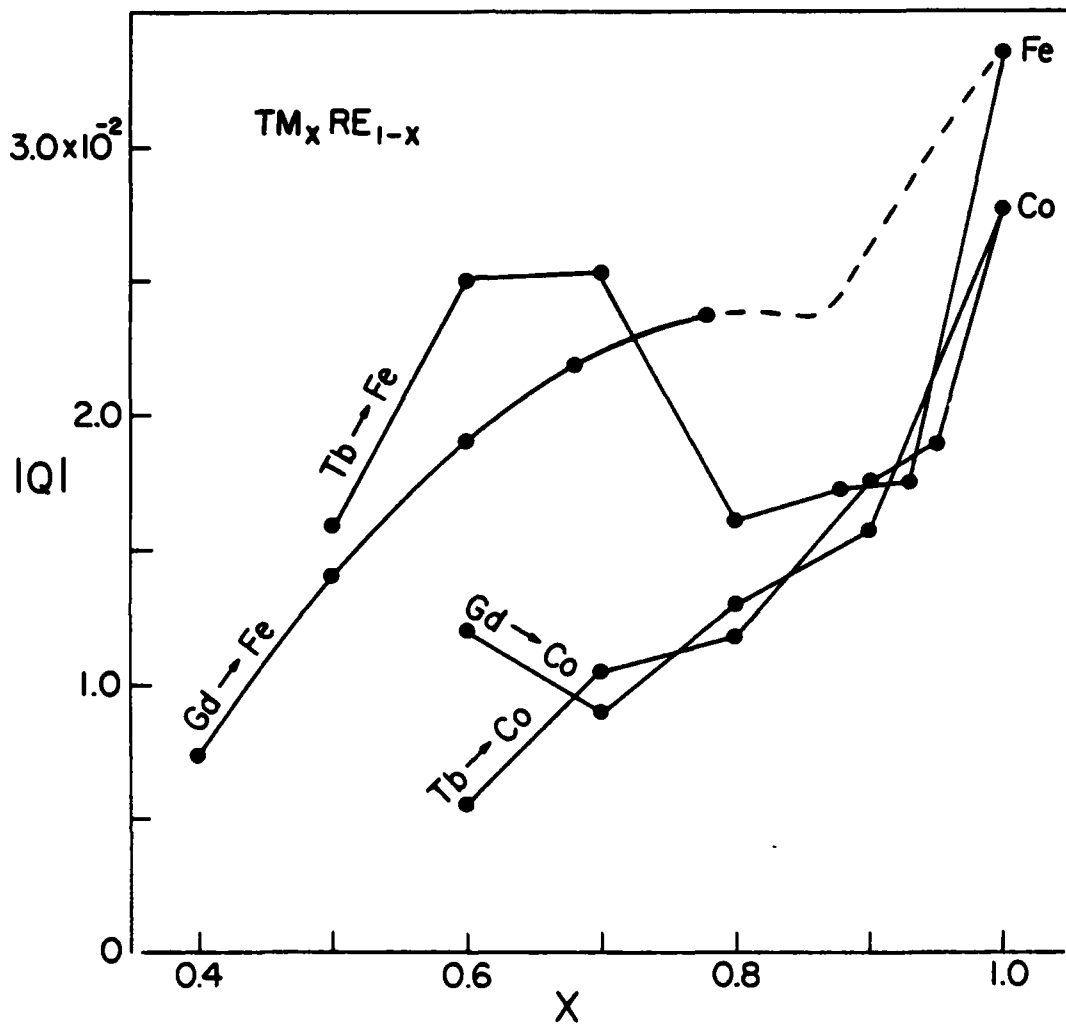


Figure 6

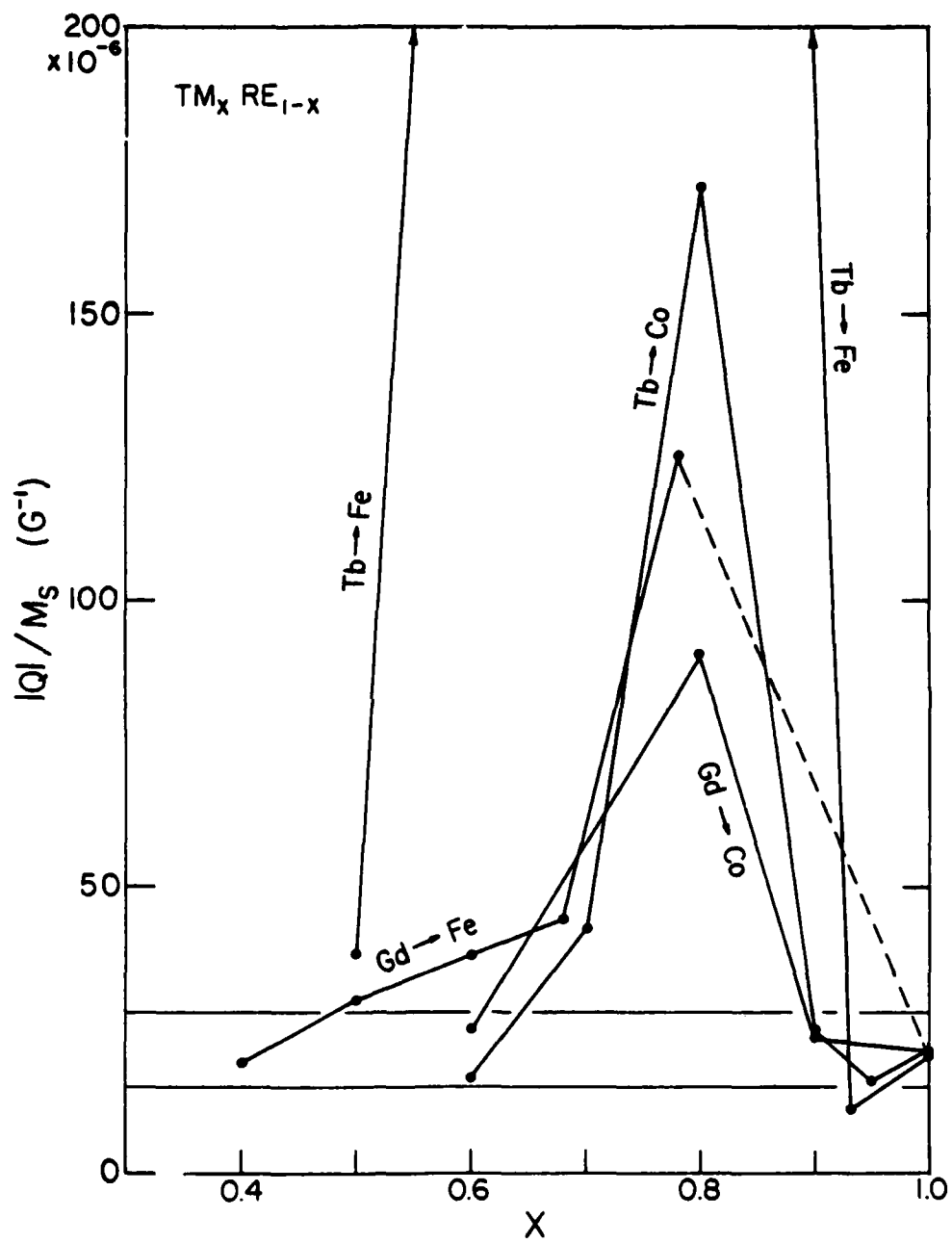


Figure 7

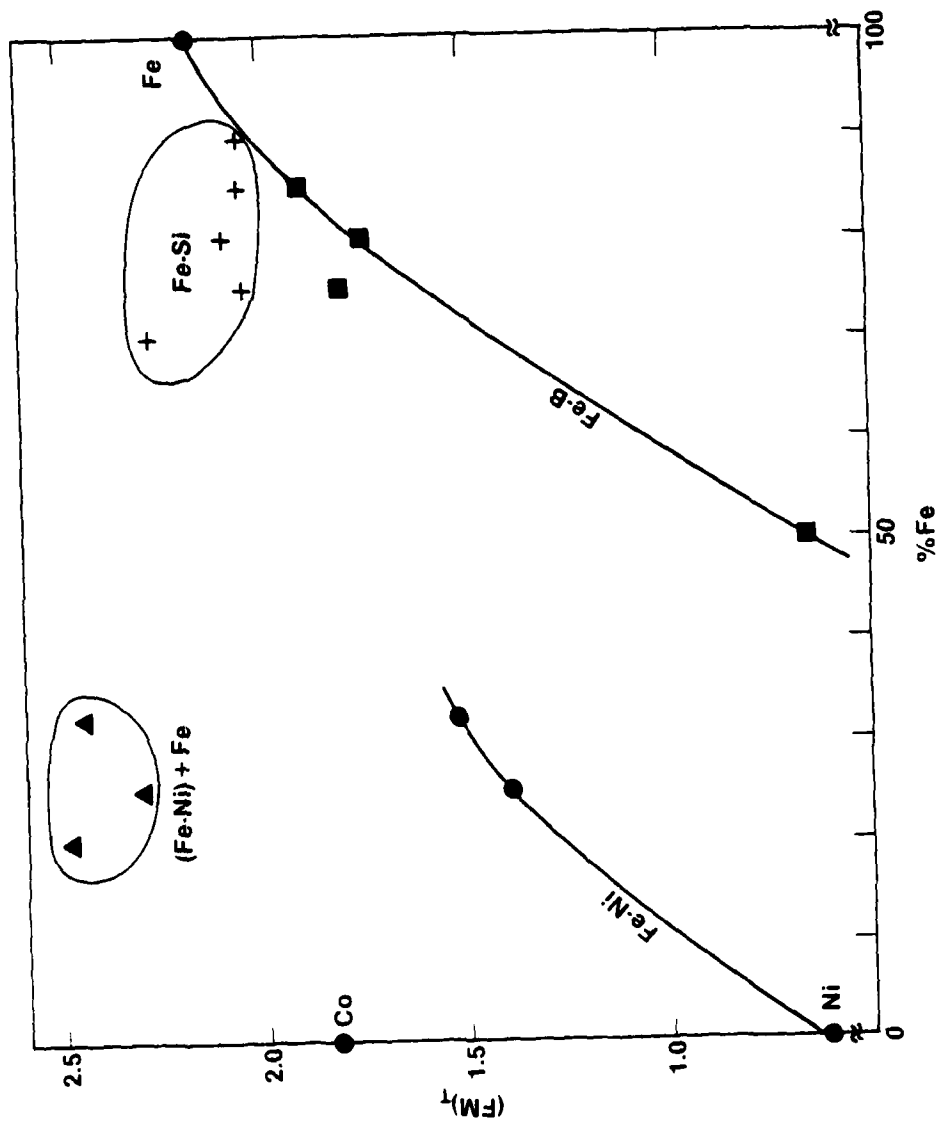


Figure 8

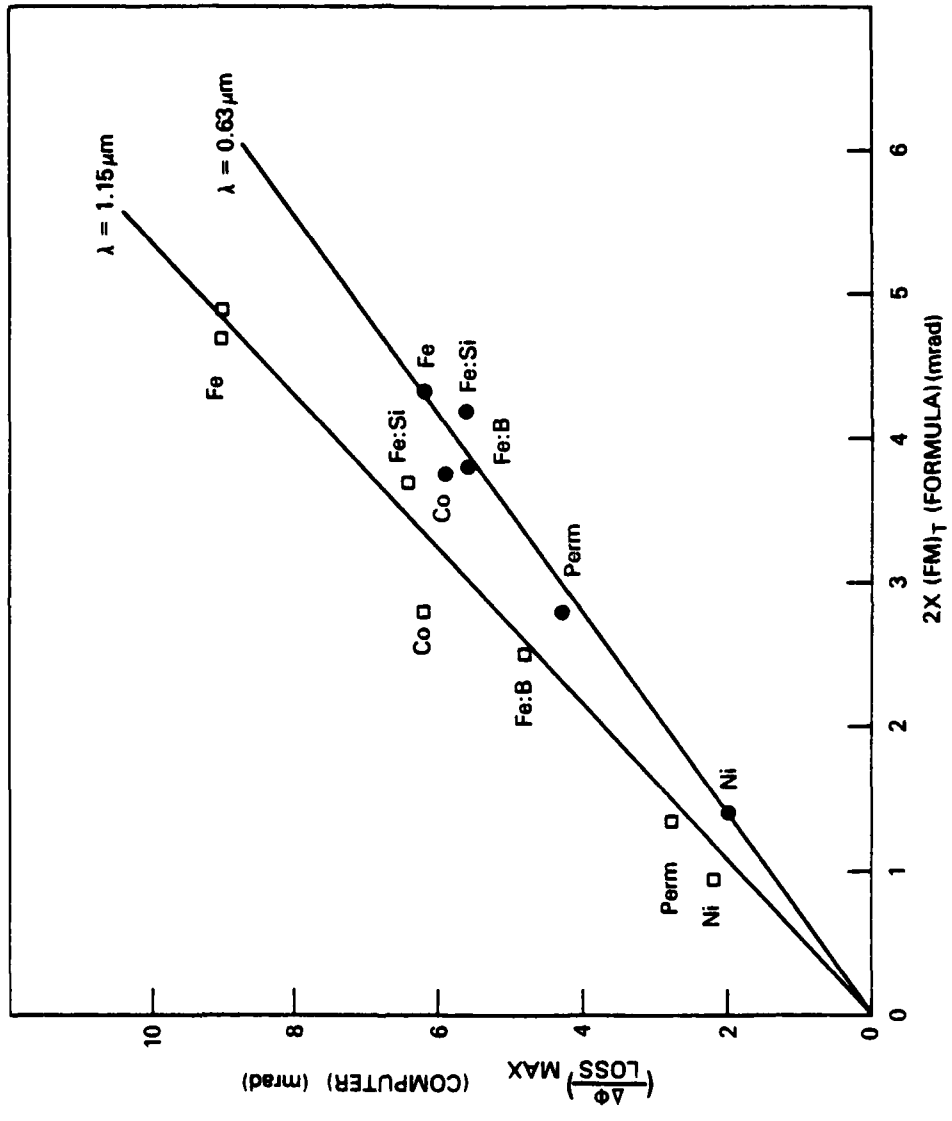


Figure 9

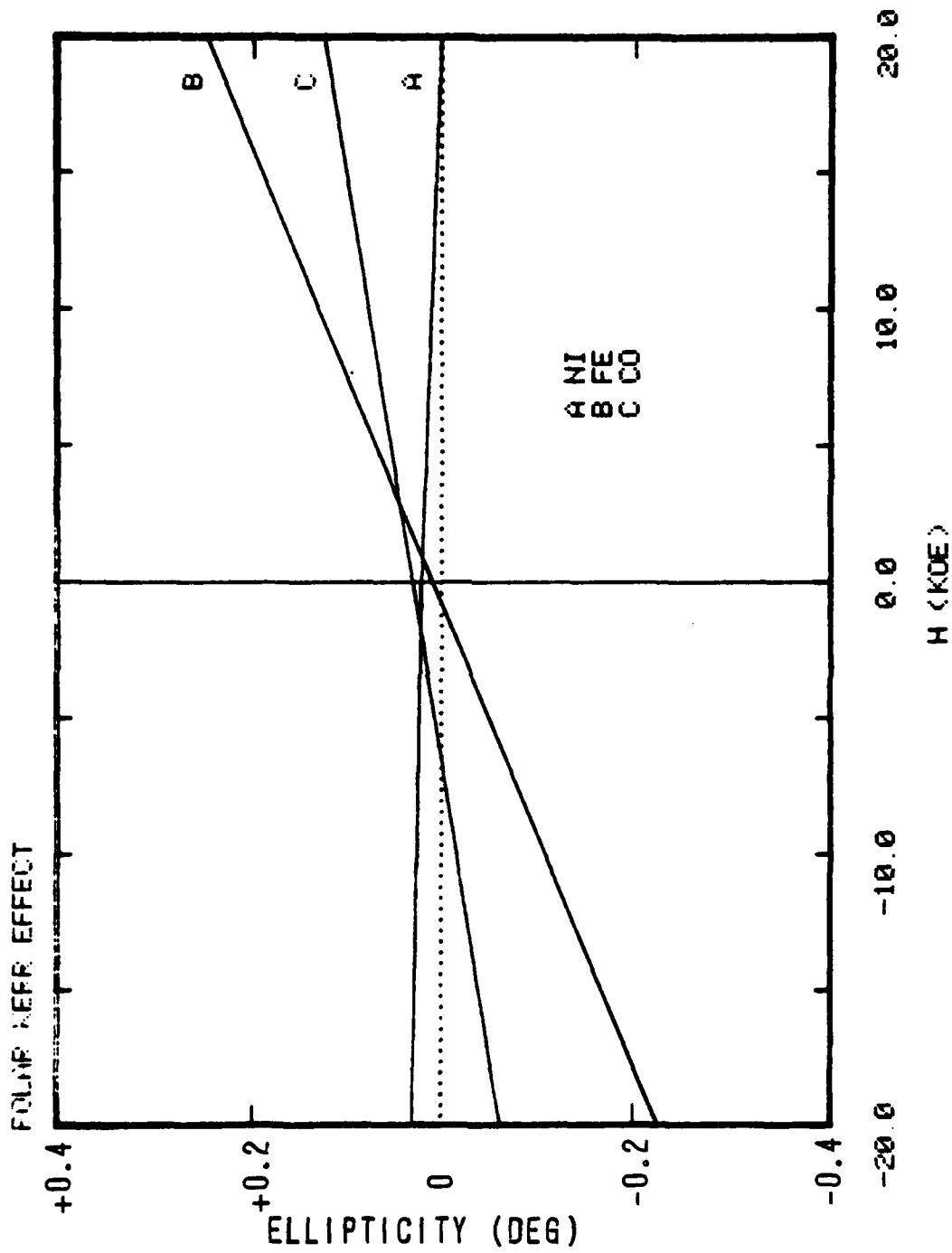
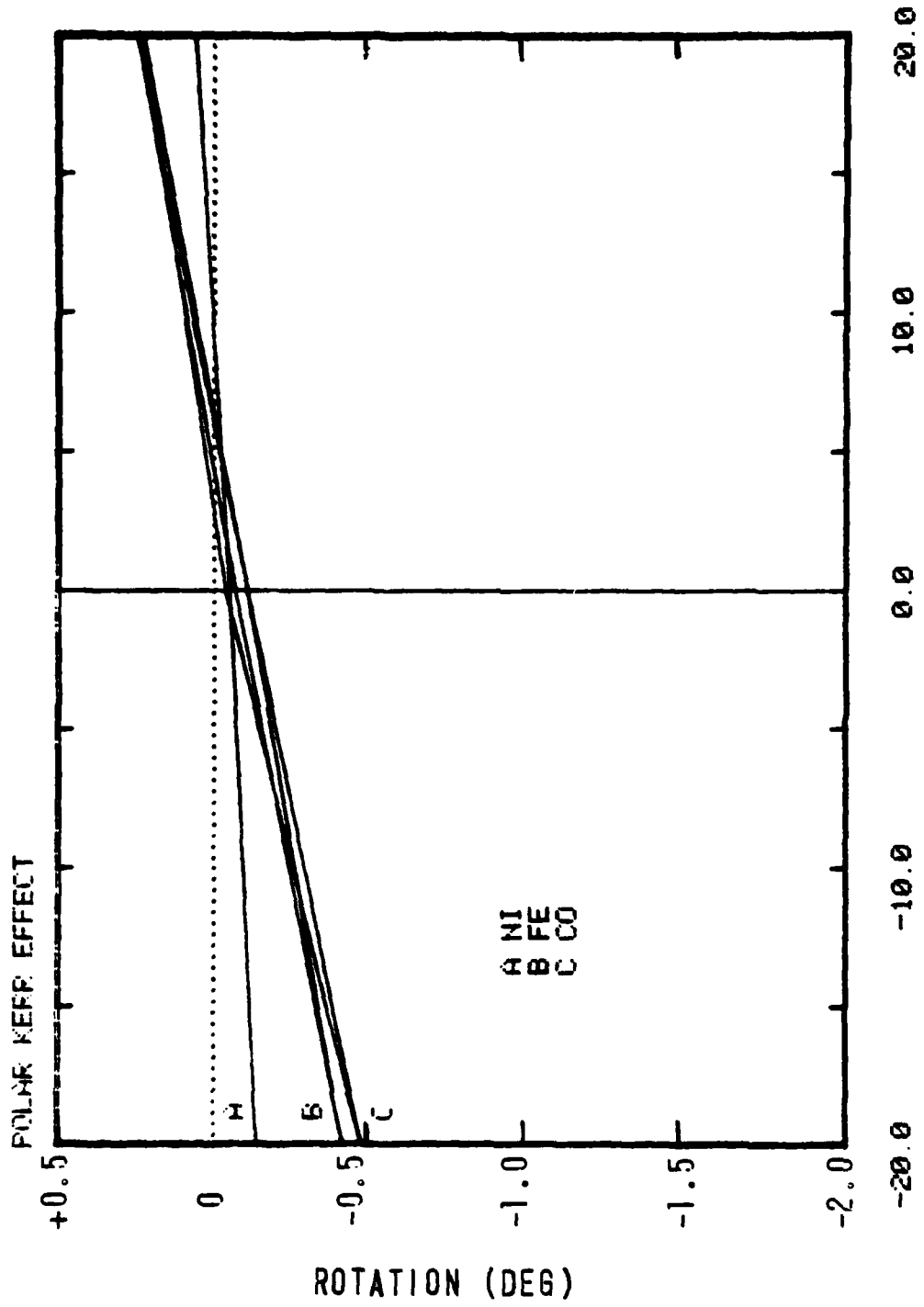


Figure 10



H (KOE)  
Figure 11

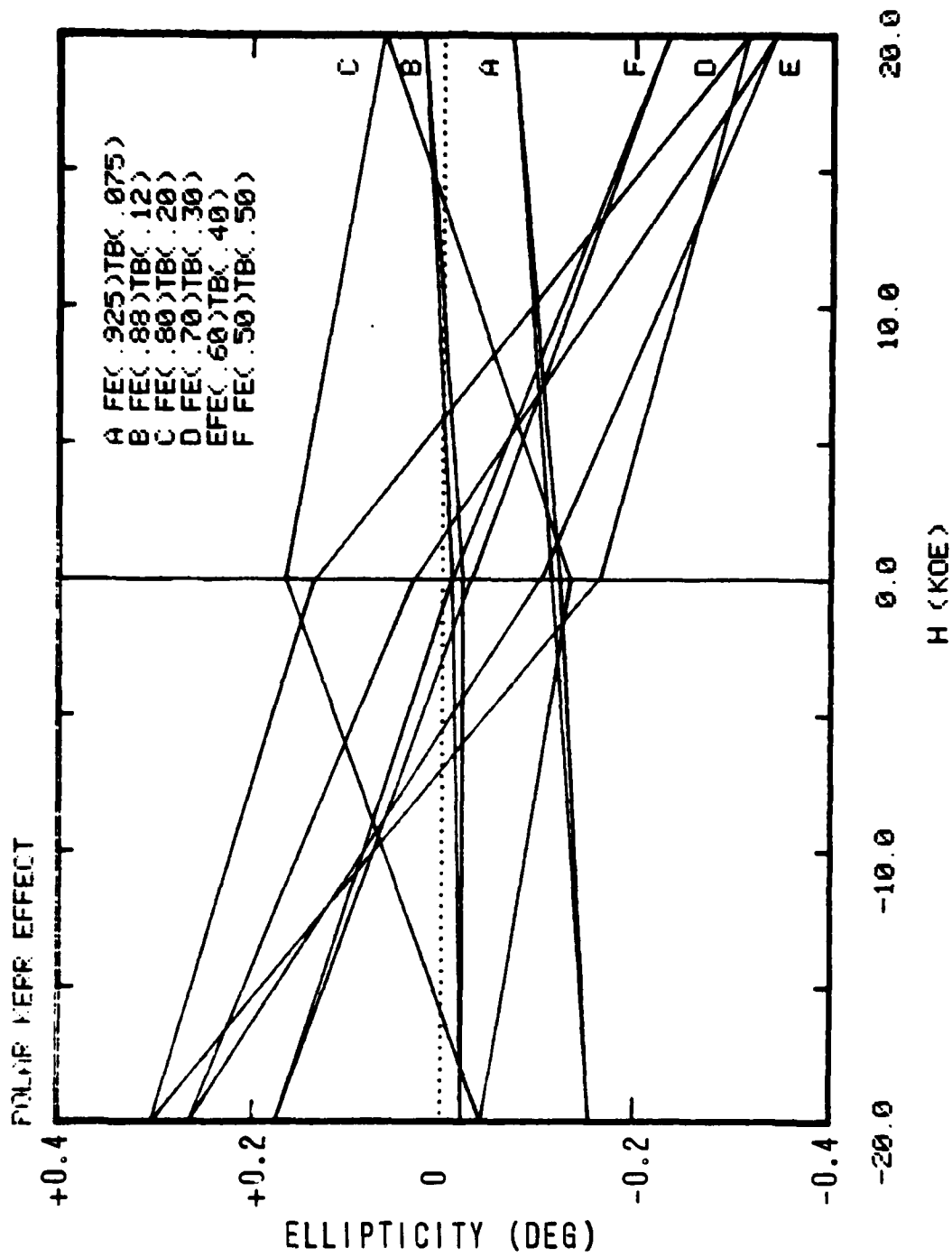
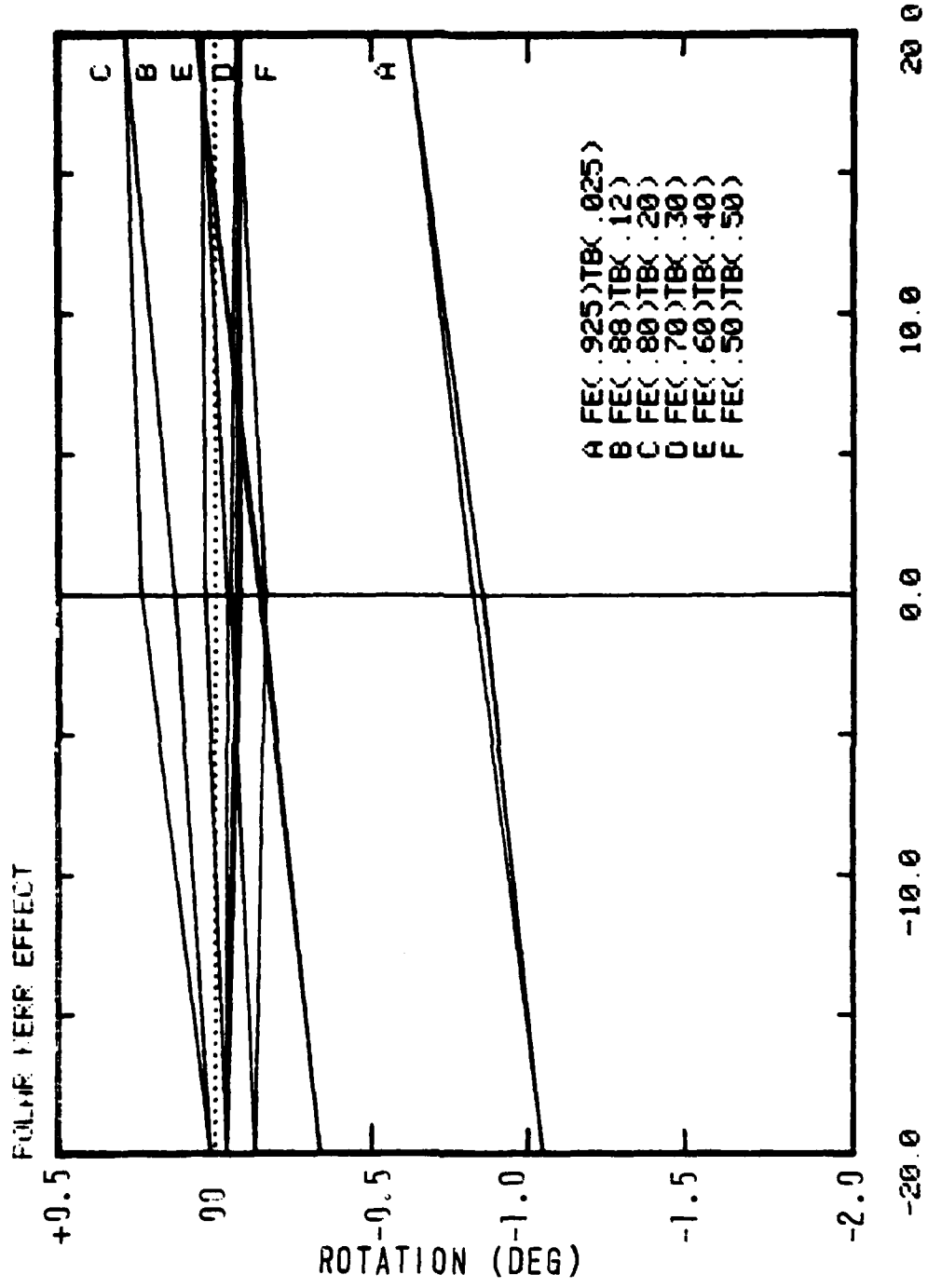
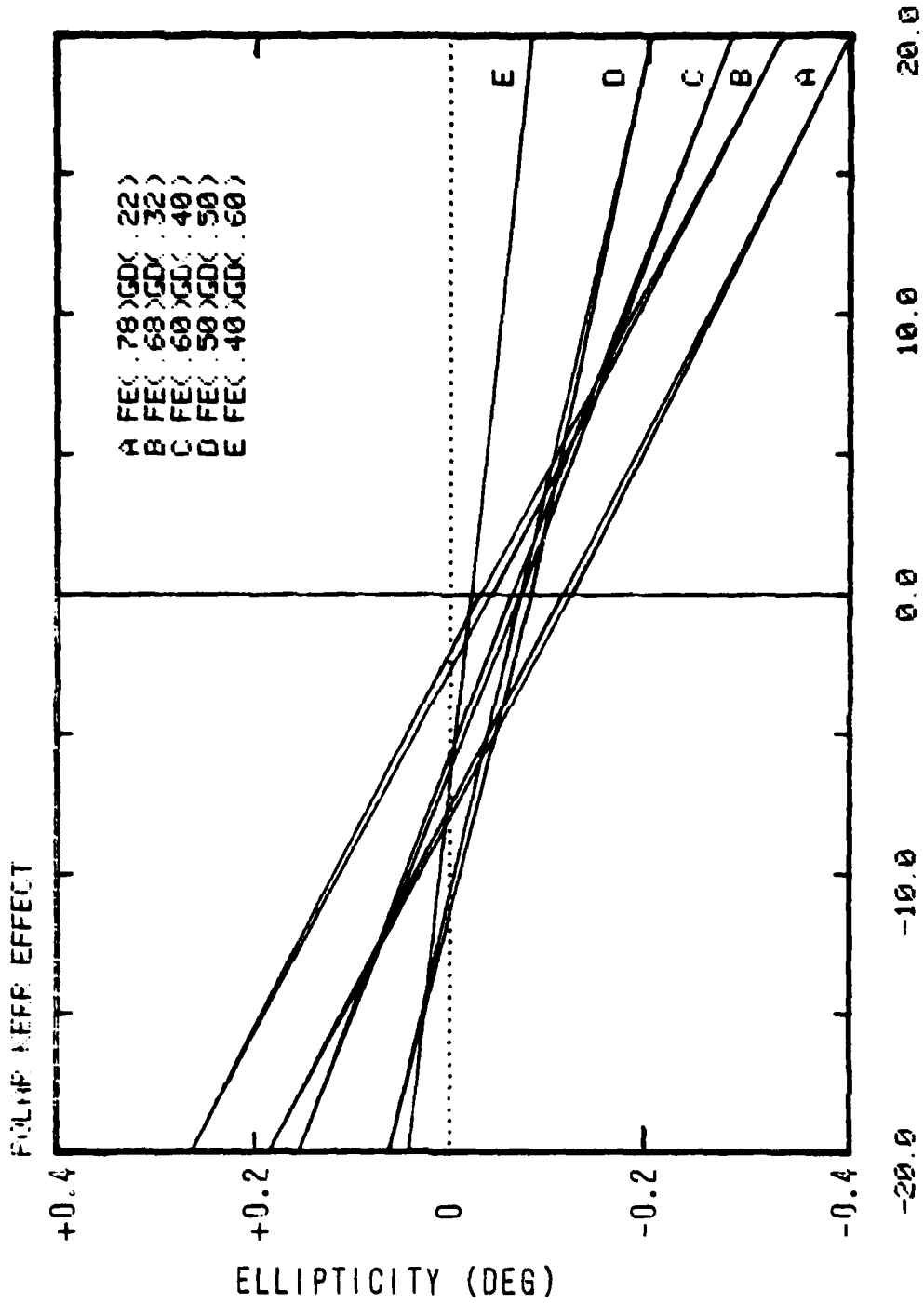


Figure 12

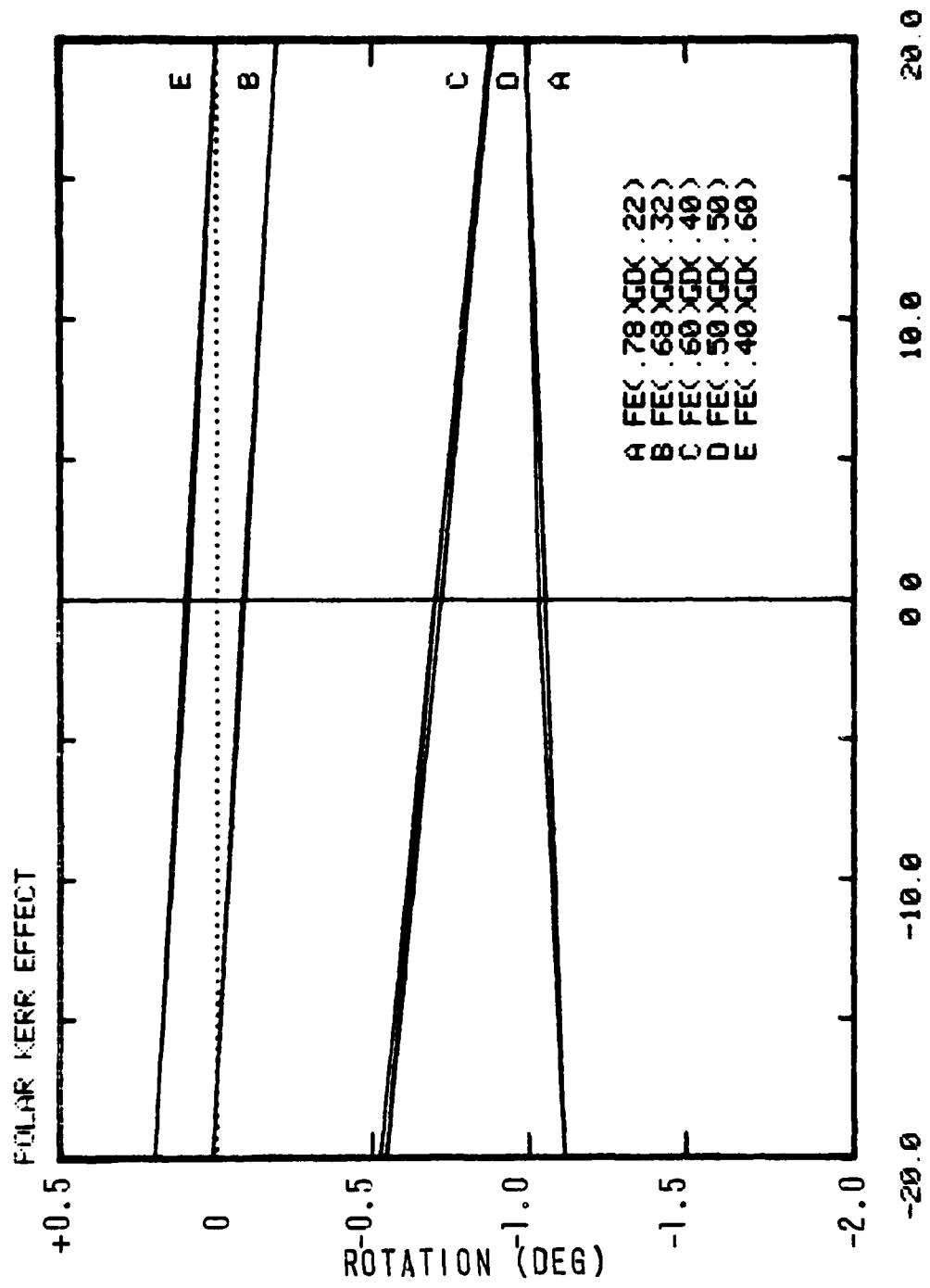


H (KOE)

Figure 13



H (KOE)  
Figure 14



H (KOE)  
Figure 15

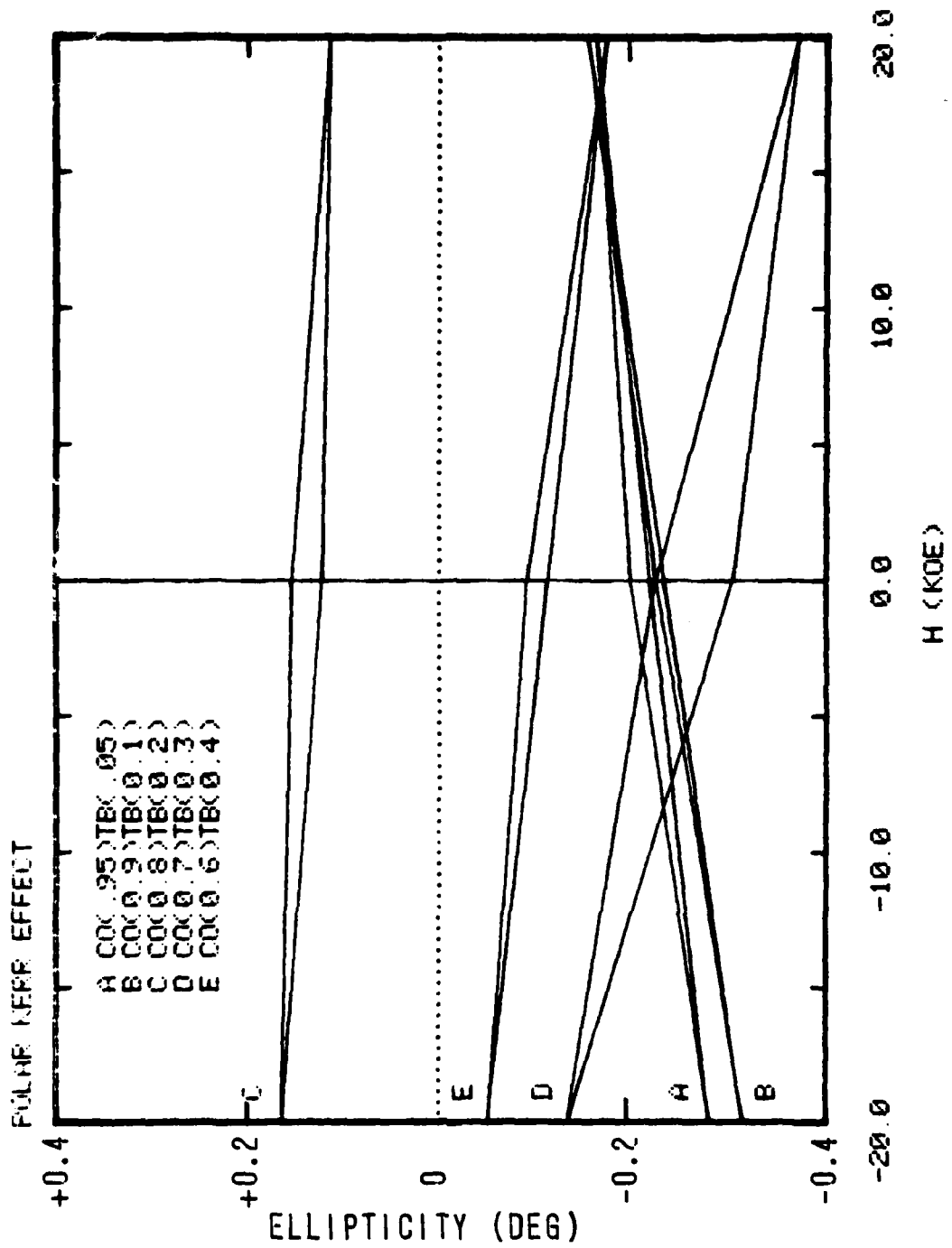


Figure 16

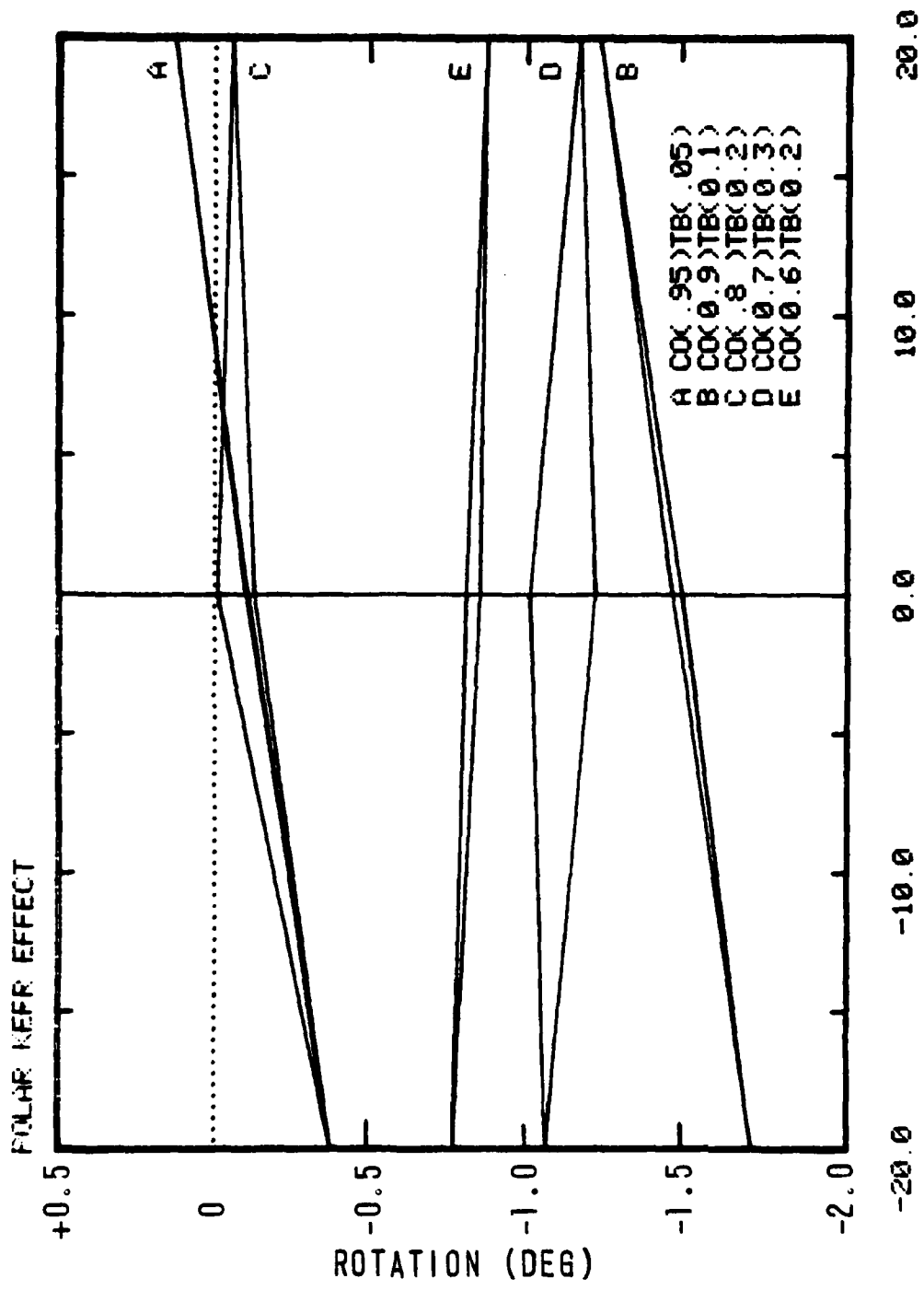


Figure 17

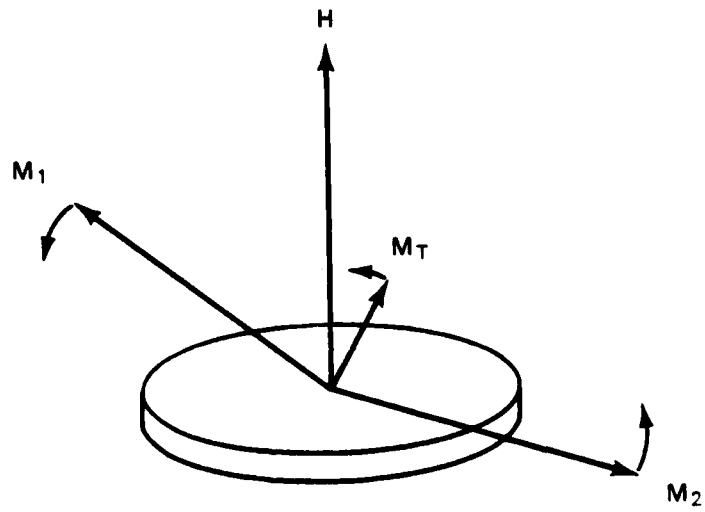


Figure 18

Table I

## OPTICAL AND MAGNETO-OPTICAL DATA

SAMPLE	n	k	Q <sub>1</sub>	Q <sub>2</sub>	4πM <sub>s</sub> (kG)	Q <sub>1</sub> /M <sub>s</sub> (10 <sup>-6</sup> G <sup>-1</sup> )
			(10 <sup>-3</sup> )	(10 <sup>-3</sup> )		
Fe	2.75	3.23	33.6	0.3	20.6	20.1
Fe-Gd(0.78,0.22) <	2.91	3.50	-10.2	-21.5	2.34	124.9
Fe-Gd(0.68,0.32)	2.47	3.09	-17.7	-12.9	6.35	43.9
Fe-Gd(0.60,0.40)	2.47	3.01	-18.2	-5.2	6.13	38.3
Fe-Gd(0.50,0.50)	2.32	2.92	-13.9	-0.9	5.90	29.9
Fe-Gd(0.40,0.60)	2.21	2.76	-7.3	+0.4	4.67	18.8
Fe-Tb(0.93,0.07)	3.27	3.38	+15.1	-9.0	4.02	5.5
Fe-Tb(0.88,0.12)	3.19	3.85	+14.7	-9.0	0.66	335.6
Fe-Tb(0.80,0.20)	2.93	3.60	+14.9	-6.0	-	-
Fe-Tb(0.70,0.30) <	2.99	3.61	-13.2	-21.6	0.67	477.5
Fe-Tb(0.60,0.40)	3.00	3.59	-12.0	-21.9	-	-
Fe-Tb(0.50,0.50)	2.86	3.45	-10.7	-11.7	5.36	38.2
Co	2.25	3.64	+26.8	-6.9	16.8	20.9
Co-Gd(0.90,0.10)	2.41	3.31	(+14.5)	(-6.1)	8.5	23.2
Co-Gd(0.80,0.20)	2.88	3.63	+8.6	-9.8	1.9	89.0
Co-Gd(0.70,0.30) <	2.81	3.38	(-6.4)	(+6.2)	-	-
Co-Gd(0.60,0.40)	2.96	3.48	-12.0	+1.6	6.0	25.5
Co-Tb(0.95,0.05)	2.46	3.41	+18.0	-6.5	14.92	16.0
Co-Tb(0.90,0.10)	2.37	3.11	+17.0	-4.7	9.12	24.2
Co-Tb(0.80,0.20)	2.40	3.17	+8.9	-6.8	0.85	172.4
Co-Tb(0.70,0.30) <	2.53	3.07	-8.9	-5.4	2.78	42.6
Co-Tb(0.60,0.40)	2.55	3.00	-5.3	-1.3	3.84	16.7
Co-Sm(0.90,0.10)	2.38	2.86	+7.8	-7.2	-	-
a Co-Sm(0.83,0.17)	2.38	3.13	+13.1	-6.6	-	-
b Co-Sm(0.83,0.17)	2.30	3.03	+13.3	-8.8	-	-
Co-Sm(0.60,0.40)	2.92	2.87	-0.5	-4.8	-	-

Values of Q<sub>1</sub>, Q<sub>2</sub> in parentheses were not in saturated state. a,b are independent samples.  
 < indicates the approximate compensation composition.

Table II  
Transverse Kerr Effect

Material	$\lambda = 0.63 \mu\text{m}$					$\lambda = 1.15 \mu\text{m}$				
	n	k	$Q_1$	$Q_2$	(FM) $_T$ (mrad)	n	k	$Q_1$	$Q_2$	(FM) $_T$ (mrad)
Fe	2.73	3.23	.034	.000	2.17	3.71	5.14	.028	-.059	2.41
Ni	1.80	3.24	.006	-.004	.70	3.23	6.13	.001	.014	.48
Co	2.25	3.64	.026	-.005	1.83	4.42	6.61	.030	-.046	1.40
Fe (.85) B (.15)	3.10	3.64	.033	-.011	1.90	4.77	5.46	.000	-.044	1.27
Fe (.90) Si (.10)	2.60	2.96	.029	.002	2.10	3.82	4.98	.018	-.047	1.86
Fe (.25) Ni (.75)	2.16	3.35	.015	-.011	1.40	4.08	5.57	.018	-.026	1.00
Fe (.25) Ni (.75) + 250 Å Fe	3.06	3.39	.038	-.012	2.30	3.99	5.84	.017	-.014	.69

Table III  
Magnetization Normal to Plane

<u>Sample</u>	<u><math>4\pi M_s</math></u>	<u><math>4\pi M_R</math></u>	<u><math>H_c</math> (Oe)</u>
Co-Tb (0.95,0.05)	14,920	746	625
Co-Tb (0.9,0.1)	9,120	746	750
Co-Tb (0.8,0.2)	850	850	8,600
Co-Tb (0.7,0.3)	2,780	2,518	5,250
Co-Tb (0.6,0.4)	3,840	1,840	1,700
Fe-Gd (0.78,0.22)	2,340	470	550
Fe-Gd (0.68,0.32)	6,350	490	500
Fe-Gd (0.6,0.4)	6,130	460	550
Fe-Gd (0.5,0.5)	5,900	640	560
Fe-Gd (0.4, 0.6)	4,670	< 100	< 100
Co	16,800	$\sim 0$	$\sim 0$
Fe-Tb (0.93,0.07)	4,020	375	600
Fe-Tb (0.88,0.12)	660	160	1,400
Fe-Tb (0.8,0.2)	—	(Compensation)	—
Fe-Tb (0.7,0.3)	670	< 50	< 50
Fe-Tb (0.5,0.5)	5,360	450	600
Co-Gd (0.9,0.1)	8,500	540	560
Co-Gd (0.8,0.2)	1,900	< 100	< 100
Co-Gd (0.7,0.3)	—	(Compensation)	—
Co-Gd (0.6,0.4)	6,000	415	500